THE JOURNAL OF PHYSICAL CHEMISTRY B

ARTICLE

pubs.acs.org/JPCB

Coupling between Electron Transfer and Protein−Solvent Dynamics: FTIR and Laser-Flash Spectroscopy Studies in Photosynthetic Reaction Center Films at Different Hydration Levels

Marco Malferrari,[†] Francesco Francia,[†] and Giovanni Venturoli*[,†,‡]

[†]Laboratorio di Biochimica e Biofisica, Dipartimento di Biologia, Università di Bologna, 40126 Bologna, Italy

[‡]Consorzio Nazionale Interuniversitario per le Scienze Fisiche della Materia, c/o Dipartimento di Fisica, Università di Bologna, 40127 Bologna, Italy

ABSTRACT: We report on the relationship between electron transfer, conformational dynamics, and hydration in photosynthetic reaction centers (RCs) from *Rhodobacter sphaeroides*. The kinetics of electron transfer from the photoreduced quinone acceptor (Q_A^-) to the photo-oxidized primary donor (P^+), a charge recombination process sensitive to the conformational dynamics of the RC, has been analyzed at room temperature in dehydrated RC−detergent films as a function of the residual water content under controlled relative humidity (r). The hydration level was evaluated by FTIR spectroscopy from the area of the combination band of water (5155 cm^{-1}). Sorption isotherms fit the Hailwood and Horrobin model and indicate a significant contribution to hydration of the detergent belt surrounding the RC. Spectral analysis of the water combination and association (2130 cm^{-1}) bands suggests strong rearrangements in the hydrogen-bonding organization upon depletion of the hydration shell of the complex. In parallel with these changes, following dehydration below a critical threshold ($r \cong 40\%$), the kinetics of $P^+Q_A^-$ recombination become progressively faster and distributed in rate. When r is decreased from 40% to 10% the average rate constant $\langle k \rangle$ increases from 15 to 40 s^{-1}, mimicking the behavior of the hydrated system at cryogenic temperatures. We infer that extensive dehydration inhibits dramatically the relaxation from the dark- to the light-adapted conformation of the RC as well as interconversion among lower tier conformational substates. The RC dynamics probed by $P^+Q_A^-$ recombination appear therefore controlled by the thermal fluctuations of the hydration shell. At $r < 10\%$ an additional, much faster ($\langle k \rangle \cong 3000$ s^{-1}) kinetic phase of $P^+Q_A^-$ recombination is observed. We suggest such a fast recombination arises from removal of a pool of RC-bound water molecules which are essential to stabilize the primary charge-separated state at physiological conditions.

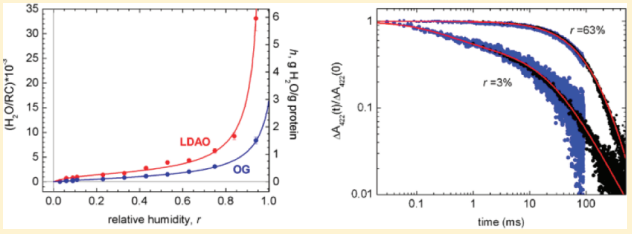

1. INTRODUCTION

Many of the diverse functions of proteins involve a large variety of thermally activated internal motions, spanning a time window which extends over many orders of magnitude.[1] These complex dynamics originate from rugged energy landscapes which feature many quasi-isoenergetic local minima corresponding to different conformational substates, organized hierarchically in tiers.[2,3] Inasmuch as myoglobin (Mb) can be regarded as an established paradigm to study function−dynamics relationships in soluble proteins,[4] the bacterial photosynthetic reaction center (RC) is becoming a prototype when approaching analogous problems in integral membrane proteins.[5,6] This large pigment−protein complex, which catalyzes the primary photochemical events of solar-energy conversion in photosynthetic bacteria, offers unique advantages when investigating the connection between conformational dynamics and one of the simplest, largely widespread biocatalytic events, i.e., intraprotein electron transfer.

Within the RC of *Rhodobacter* (*Rb.*) *sphaeroides*, following absorption of a photon, a bacteriochlorophyll special pair (P) acts as the primary electron donor, delivering an electron, via an intermediate bacteriopheophytin (BPhe) molecule, to a ubiquinone-10 electron acceptor (Q_A), generating in ∼200 ps the primary charge-separated state $P^+Q_A^-$ (for reviews see refs 7 and 8). The electron is then transferred to the secondary ubiquinone-10 acceptor (Q_B). In the isolated RCs, in the absence of electron donors to P^+, the electron on Q_B^- recombines with the hole on P^+. In Q_B deprived RCs or in the presence of inhibitors of the Q_A^- to Q_B electron transfer, charge recombination occurs by direct electron tunneling[9] from Q_A^- to P^+.

Many experimental observations point to a tight connection between the RC dynamics and single electron transfer steps catalyzed by the RC from the picosecond charge separation between P and the BPhe intermediate acceptor[10] to the microsecond electron transfer from the photoreduced Q_A^- to Q_B, which has been shown to be a conformationally gated process.[11] The emerging concept is that the RC protein behaves as an inhomogeneous

Received: June 20, 2011
Revised: October 12, 2011
Published: October 21, 2011

dx.doi.org/10.1021/jp2057767 | *J. Phys. Chem. B* 2011, 115, 14732–14750

solvent, which relaxes upon charge separation over different time scales,[5,12−18] thus participating in the function and regulation[19,20] of the RC. Structural changes revealed by X-ray diffraction studies have been associated to charge separation, including a substantial movement of Q_B upon its reduction to semiquinone, detected in crystals of *Rb. sphaeroides* RC illuminated at room temperature before freezing,[21] and a concerted movement of the H subunit after prolonged illumination.[22] More recently, a light-induced conformational change, involving the side chain of a tyrosine residue close to P, has been caught by time-resolved Laue diffraction in the RC from the related species *Blastochloris viridis*.[6]

Basic information on the conformational RC dynamics has been gained by studying the low-temperature kinetics of $P^+Q_A^-$ recombination following a short flash of light. As originally shown by Kleinfeld et al.[13] the electron transfer from Q_A^- to P^+ is accelerated by a factor of ∼5, as compared to room temperature, when RCs are frozen to 77 K in the dark, whereas it is sizably slowed when RC are cooled in the light. This observation revealed that the RC can be trapped at low temperature in a dark-adapted or light-adapted conformation, substantially differing in the stability of the charge-separated state. Furthermore, as indicated by the strongly nonexponential, distributed kinetics of $P^+Q_A^-$ recombination at cryogenic temperatures, both conformations consist of a large ensemble of lower tier conformational substates. The temperature dependence (300−5 K) of $P^+Q_A^-$ has been examined systematically by McMahon et al.,[5] who analyzed the coupling between the RC dynamics and this electron transfer process within the frame of a quantum mechanical spin-boson model. According to their dynamical model, at room temperature, the RC protein relaxes rapidly to the light-adapted conformation by solvating the altered charge distribution, thus decreasing the energy gap between $P^+Q_A^-$ and the PQ_A ground state. At room temperature the RC protein also samples rapidly the ensemble of its conformational substates, averaging structural and kinetic heterogeneities over the time scale of charge recombination. The above processes (fast thermal fluctuations and relaxation) result in the relatively slow ($\tau \approx 100$ ms) and exponential $P^+Q_A^-$ recombination. When RC are frozen in the dark between 250 and 150 K both thermal averaging and the relaxation from the dark- to the light-adapted conformation are hampered giving rise to the observed distributed and accelerated kinetics of charge recombination. The kinetics of this electron transfer process provides therefore a simple, sensitive probe of RC dynamics.

Besides low-temperature investigations a valuable approach to study the interplay between electron transfer and protein dynamics consists in examining the effects of dehydration at room temperature. This complementary strategy can provide additional information, disentangling temperature from matrix effects, and clarifying the relationship between internal motions of the protein and the dynamics of its solvent environment. In fact, the last decades of experimental and theoretical work on soluble proteins have led to the idea that solvent fluctuations dominate protein dynamics and functions, which are arrested below critical levels of hydration.[23−25] It has been proposed, in particular, that small-scale internal motions, which involve side chains of the protein and govern processes such as ligand migration between different cavities inside Mb, are driven and controlled by the fast fluctuations of water interacting with the protein, forming the so-called hydration shell.[26] These water molecules exhibit structural and dynamical properties distinct from those of bulk water.[27−30]

In the case of the RC, a pioneering study by Clayton[31] indicated that air-dried RC films partially retained primary photochemistry but exhibited an accelerated charge recombination. Dehydration of membrane fragments (chromatophores) of *Rhodospirillum rubrum* was reported to impair Q_A^- to Q_B electron transfer as a result of the loss of water molecules which were considered strongly bound to the RC.[32] More recently, we studied systematically the effect of dehydration on the room-temperature kinetics of $P^+Q_A^-$ recombination in RCs incorporated into trehalose glassy matrices. The results[33−37] show that dehydration of the system below a critical level inhibits the RC relaxation which stabilizes the charge-separated state and hinders interconversion among conformational substates: the restriction of these RC dynamics is comparable to that observed at cryogenic temperatures. In light of experimental results and molecular dynamics (MD) simulations in trehalose−water matrices incorporating Mb or RC complexes we proposed that inhibition of protein dynamics observed in both systems at low water contents is mediated by residual water molecules of the protein hydration shell which bridge protein surface groups with trehalose molecules of the matrix by forming a network of multiple hydrogen bonds.[38] The ability of the glassy matrix to control the RC dynamics at low hydration levels is therefore brought back to its efficacy in retarding the dynamics of the hydration shell to which the conformational dynamics probed by the electron transfer kinetics are thought to be slaved.[35−37] If this scenario is correct we expect that depletion of the hydration shell of the protein in the absence of any embedding matrix is able per se to inhibit the RC dynamics, leading, at sufficiently low water contents, to a strong retardation of the RC internal motions coupled to $P^+Q_A^-$ recombination. The main aim of the present work was to test this expectation by analyzing the kinetics of $P^+Q_A^-$ recombination in RC−detergent films over a large range of controlled hydration levels. Fourier transform infrared (FTIR) spectral analysis of the combination (5155 cm^{-1}) and association (2130 cm^{-1}) bands of water allowed us to estimate the water content of the films even at very low hydration, to construct water sorption isotherms, and to correlate the effects observed on the electron transfer kinetics with structural/dynamical properties of the residual hydration shell of the complex. The results, obtained in the presence of two different detergents, indicate that dehydration of the complex retards the RC thermal fluctuations and relaxations probed by the kinetics of $P^+Q_A^-$ recombination, mimicking at room temperature effects observed at cryogenic temperatures in the hydrated system. Furthermore, data at extremely low hydration suggest that a limited number of tightly bound water molecules is essential to stabilize the primary, light-induced charge-separated state on the time scale of 10^{-2} s.

2. MATERIALS AND METHODS

2.1. RC Purification and Sample Preparation. RCs extracted from *Rb. sphaeroides* strain 2.4.1 membranes using lauryldimethylamine *N*-oxide (LDAO) as detergent were purified essentially as described in ref 39. To replace the detergent LDAO with *n*-octyl β-D-glucopyranoside (OG) the LDAO suspension of purified RCs, eluted from the DEAE column (DE52, Whatman), was dialyzed twice for 10 h against a 100 times larger volume of 10 mM Tris buffer, pH 8.0 in the presence of 0.1% OG rather than 0.025% LDAO. LDAO and OG were from Sigma-Aldrich and Anatrace (Maumee, OH, USA), respectively. The samples employed for FTIR absorption measurements were RC films

prepared according to the following procedure. A drop (0.168 mL) of the dialyzed RC−detergent solution at 60 μM RC concentration, in the presence of 10 mM *o*-phenanthroline and 0.025% LDAO or 0.1% OG, was deposited at the center of a 50 mm diameter CaF_2 window and dried in a desiccator for about 4 h under N_2 flow at room temperature.

Different hydration levels of the RC−detergent films were obtained by equilibrating the samples with hydrating saturated solutions providing defined values of relative humidity, *r*. To this end the window on which the RC film was formed was inserted into a specifically designed sample holder, equipped with a second CaF_2 window, to form a gas-tight cylindrical cavity (volume ≅ 7.7 mL), which contained at the bottom about 1.5 mL of the hydrating solution. The following saturated solutions were employed to obtain the desired relative humidity (indicated in brackets)[40] at 297 K: KNO_3 (94%), KCl (84%), NaCl (75%), NH_4NO_3 (63%), $Mg(NO_3)_2$ (53%), K_2CO_3 (43%), $MgCl_2$ (33%), CH_3COOK (23%), LiCl (11%), $KOH\cdot 2H_2O$ (9%), $NaOH\cdot H_2O$ (6%), P_2O_5 (3%). Spectroscopic measurements were performed directly on the film exposed to the saturated atmosphere inside the holder. This allowed us to monitor directly the time course of water sorption/desorption during equilibration of the RC film by following the evolution of the NIR water combination band at about 1940 nm (see Results). When the relative humidity inside the holder was varied over the explored range (3% ≤ *r* ≤ 94%), a steady hydration level was reached in a few hours. After replacement of the hydrating solution in the holder, RC−detergent films were always allowed to equilibrate for a minimum of 15 h.

2.2. Spectroscopic Measurements. FTIR absorption measurements were performed at 297 K using a Jasco Fourier transform 6100 spectrometer, equipped with a DLATGS detector. Spectra in the mid-IR range (7000−1000 cm^{-1}) were acquired using a standard high-intensity ceramic source. Measurements were extended to the NIR region (15 000−2200 cm^{-1}) using a halogen lamp source, replacing the Ge/KBr with a Si/CaF_2 beam splitter and the KRS-5 with a CaF_2 exit interferometer window. Occasionally FTIR spectra were also recorded with a Bruker Tensor 27 spectrometer. The spectra were recorded with a resolution of 4 cm^{-1}, adding 10^2 and 10^3 scans per spectrum in samples equilibrated at $r > 11\%$ and $r \leq 11\%$, respectively.

Decomposition of absorption bands into Gaussian components as well as fitting of hydration data to sorption isotherms was performed by nonlinear least-squares minimization using Origin (Microcal Software, Northampton, MA, USA). Confidence intervals of the fitting parameters were evaluated numerically through an exhaustive search method, as described in detail in ref 36 using routines written in LabTalk language (Origin).

The recombination kinetics of $P^+Q_A^-$ following flash excitation were recorded at 422 and 450 nm[41] using an apparatus for time-resolved absorption spectroscopy of local design, essentially as described in ref 35. The relative contribution of P^+ and Q_A^- to the absorption change at 422 and 450 nm can be evaluated from the differential extinction coefficients for P^+/P and Q_A^-/Q_A at the two wavelengths. By using the spectral data of ref 41 and extinction coefficients[42,43] $\varepsilon_{605}(P^+/P) = 19.5\ mM^{-1}\ cm^{-1}$ and $\varepsilon_{450}(Q_A^-/Q_A) = 8.5\ mM^{-1}\ cm^{-1}$, we estimated $\varepsilon_{450}(P^+/P) = 13.1\ mM^{-1}\ cm^{-1}$, $\varepsilon_{422}(P^+/P) = 28.8\ mM^{-1}\ cm^{-1}$, and $\varepsilon_{422}(Q_A^-/Q_A) = 4.9\ mM^{-1}\ cm^{-1}$. These values imply a relative contribution of Q_A^- to the flash-induced absorbance change measured at 422 and 450 nm of 14.5% and 39.4%, respectively.

The excitation flash eliciting RC photochemistry was provided by a dye laser (RDP-1; Radiant Dyes GmbH, Wermelskirchen, Germany) pumped by a frequency-doubled Q-switched Nd:YAG laser (Handy 710, Quanta System, Milano, Italy) delivering 150 mJ pulses of 7 ns width. Styryl 9 was used as a dye (λ_{max} = 810 nm); saturation of a single photoexcitation was around 85%. The CaF_2 window on which the RC−detergent films were formed, placed inside the sample holder described above, was positioned at 45° with respect to the measuring beam and to the laser excitation beam in such an orientation to minimize laser light reflection toward the detector. The photomultiplier was protected from scattered excitation light by a 0.01% blocking, 10 nm bandwidth interference filter, centered at 420 or 450 nm. When recombination kinetics exhibited fast decay phases in the 10^{-5} s time scale to avoid transient artifacts due to the scattered laser light, the photomultiplier was additionally protected by a holographic notch filter centered at 532 nm plus a Corning 4-96 glass filter. From 4 to 64 kinetic traces were averaged depending on the required time resolution and signal-to-noise ratio. During averaging the sample was allowed to dark adapt for at least 1 min between successive photoexcitations.

Fitting of $P^+Q_A^-$ recombination to model kinetics was performed by least-squares minimization routines, based on a modified Marquardt algorithm.[44] Confidence intervals of fitting parameters were evaluated numerically as described in ref 36 using locally developed software.

The integrity of the RC during aging of the RC−detergent films was checked by analyzing the Q_y absorption bands of bacteriochlorin cofactors in the 650−950 nm spectral region as described in detail in ref 35 and monitoring the extent of flash-induced $P^+Q_A^-$ charge separation.

3. RESULTS

3.1. Hydration Isotherms. The ($\nu_2 + \nu_3$) combination band of water around 1940 nm is particularly suited to evaluate the water content of the RC−detergent films. This NIR band originates from the combination of bending (ν_2 or δ−OH at 1638 cm^{-1}) and asymmetric stretching (ν_3 or ν−OH at 3000−3700 cm^{-1}) vibrations. The area under this band can be taken to be proportional to the water concentration, being unaffected, at variance with other water IR bands, by cosolvents,[45,46] by the physical state of the water sample (solid or liquid),[47] and therefore by the extent of hydrogen bonding. A proportionality constant (absorptivity) a_w = 101.9 $M^{-1}\ cm^{-1}$ nm inferred from water absorption in reverse micelles[48] was used. Since the average thickness of the RC−detergent film, i.e., the effective optical path, is not easily measured to a sufficient accuracy, we used as an internal standard the area of the amide II band of the RC (centered around 1550 cm^{-1}) . Under the assumption that the proportionality constant (absorptivity) a_{II} between the concentration of the RC and the area of this band does not depend on the hydration level of the RC−detergent film, the (H_2O/RC) molar ratio can be calculated as

$$\left(\frac{H_2O}{RC}\right) = \frac{A_w \alpha_{11}}{A_{11} \alpha_w} \qquad (1)$$

where A_w and A_{II} represent the area of the water combination band and of the amide II band, respectively. The value of a_{II} was determined from the RC absorption at 802 nm (i.e., at the peak of the Q_y band of the monomeric RC bacterichlorophyll) using an

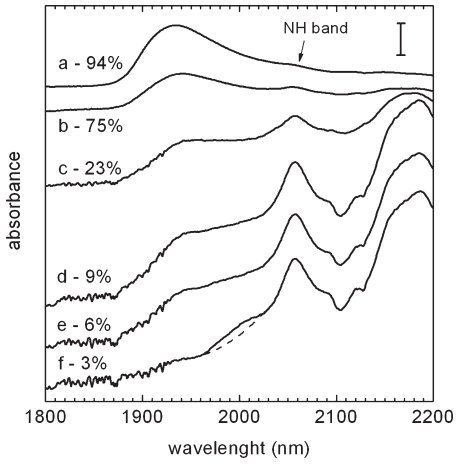

Figure 1. NIR spectra of RC−LDAO films at different hydration levels in the wavelength range of the $(\nu_2 + \nu_3)$ combination band of water. The relative humidity of the atmosphere at which the samples was exposed is indicated in the labels. The vertical bar corresponds to 40 mA for spectrum *a*, 16 mA for spectrum *b*, 5 mA for spectrum *c*, and 2 mA for spectra *d*−*f*. The dashed line shows the background of spectrum *f* in the water absorption region, evaluated as described in the text. Spectra have been normalized on the basis of the area of the amide II band.

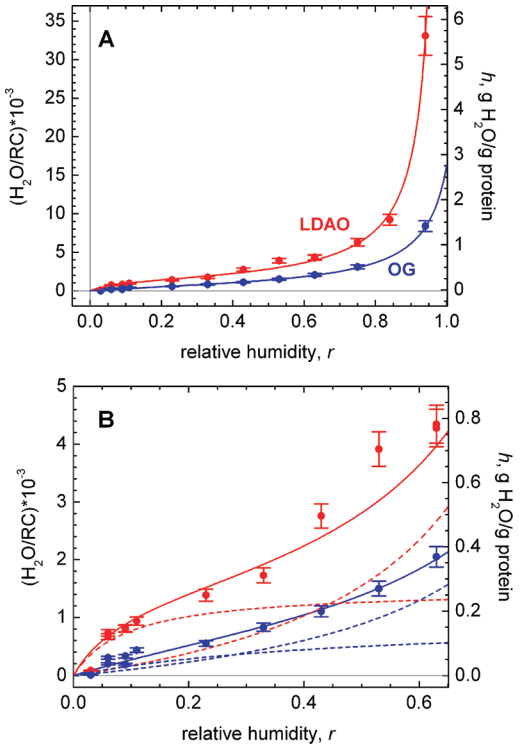

Figure 2. Hydration isotherms at 297 K determined in RC−LDAO and RC−OG films. Continuous lines represent the best fit to eq 2. The corresponding parameters are given in Table 1. (B) Enlargement of the data in panel A over the low relative humidity range. The dashed curves describe the contributions to water uptake of the two processes considered in eq 2, i.e., adsorption at strong binding sites and water condensation prevailing at high *r* values.

extinction[49] $\varepsilon_{802} = 288\ mM^{-1}\ cm^{-1}$. Spectra were collected over the 15 000−1000 cm^{-1} range in 5 freshly prepared RC−detergent films equilibrated at different relative humidity ($43\% \le r \le 94\%$) and a_{II} evaluated as $(\varepsilon_{802}\ A_{II})/A_{802}$, where A_{802} is the absorbance of the sample at 802 nm. By this approach we obtained $a_{II} = (32.7 \pm 2.8) \times 10^6\ M^{-1}\ cm^{-1}$ nm and $a_{II} = (56.6 \pm 4.3) \times 10^6\ M^{-1}\ cm^{-1}$ nm in the case of RC−OG and RC−LDAO films, respectively. The value in the presence of OG is in excellent agreement with an estimate based on spectra recorded in dried RC reconstituted into phospholipid vesicles after replacement of LDAO with OG.[50] The larger value obtained for a_{II} in RC−LDAO films can be explained by considering that the detergent LDAO contributes significantly to the IR absorption in the amide II region.[51] The a_{II} value determined in RC−LDAO films cannot therefore be considered a true value for the RC amide II absorptivity. This does not preclude, however, its correct use in eq 1, since the LDAO to RC molar ratio in the samples is fixed, being essentially determined by the number of LDAO molecules organized as a detergent belt around the hydrophobic region of the RC (see section 4.1).

Figure 1 shows FTIR spectra in the region of the water combination band measured in RC−LDAO films equilibrated at different values *r* of relative humidity, as described in section 2.1. The band is progressively reduced in amplitude when *r* decreases from 94% to 3%. Upon dehydration the band shifts to higher wavelengths and becomes narrower. The band at 2058 nm (4859 cm^{-1}), assigned to a combination[52] of the NH stretching frequency at 3280 cm^{-1} and the peptide frequency at 1550 cm^{-1}, partially overlaps with the water combination band. Under extensive dehydration, the NH band is clearly resolved, as already observed in gelatin and soluble proteins.[53] In order to correct for contributions arising from the NH band, a background spectrum has been estimated using a quadratic form to connect the regions proximal to the water band in the spectrum at $r = 3\%$ (curve *f* of Figure 1). The background spectrum (simulating the one of a fully dehydrated sample) has been subtracted from all the other spectra after normalization based on the area of the corresponding amide II bands.

The (H_2O/RC) molar ratios evaluated as described above (see eq 1) in RC−detergent films equilibrated at different relative humidity were used to construct water sorption isotherms. The films formed under nitrogen flow (see section 2.1) were characterized by (H_2O/RC) molar ratios between 1000 and 2000. Each film was first equilibrated at a relative humidity between 3% and 85%. In order to construct the isotherm, data were subsequently collected for each film at increasing relative humidity. The (H_2O/RC) molar ratios determined at a given relative humidity in different films and sorption sequences were quite reproducible and did not show any dependence upon the value of the relative humidity at which the films were initially equilibrated. No hysteresis effect was therefore observed, since each film was subjected to a desorption/sorption sequence over a different range of relative humidity. After a 3 days exposure of the RC films at room temperature the RC bacteriochlorin pigments started to lose the native coordination, as judged from the alterations in their Q_y bands (see section 2.2), particularly when the RC−detergent system was highly hydrated. Since the films were equilibrated at any value of *r* for at least 15 h, this limited the number of *r* values which could be explored in a single film: each sorption sequence included a maximum of 4 values of relative humidity. The hydration isotherms obtained by this procedure in a series of RC−LDAO and RC−OG films are shown in Figure 2. The hydration of the RC−detergent complex is given as the measured (H_2O/RC) molar ratio or as water to RC mass ratio, *h*,

dx.doi.org/10.1021/jp2057767 |*J. Phys. Chem. B* 2011, 115, 14732–14750

Table 1. Parameters of the Hailwood and Horrobin Equation (eq 2) Best Fitting the Hydration Isotherms in RC−LDAO and RC−OG Films[a]

	h_0 (g water/g protein)	h_0 (H_2O/RC) molar ratio	K_1	K_2
RC−LDAO	0.27 (0.25−0.29)	1500 (1390−1610)	10.5 (4.8−23.0)	1.02 (1.01−1.02)
RC−OG	0.18 (0.17−0.21)	1000 (944−1170)	2.0 (1.0−3.3)	0.94 (0.93−0.95)

[a] Water-to-reaction center molar ratios (H_2O/RC) have been converted into water-to-protein mass ratios by assuming a RC molecular mass of 100 KDa. Values in brackets indicate the calculated confidence intervals within one standard deviation.

assuming a molecular weight of 100 KDa for the RC. The dependence of the hydration upon r exhibits the typical sigmoidal character observed for water sorption by a number of globular and fibrillar proteins.[54,55] Over the whole r range the RC−LDAO complex is systematically more hydrated than the RC−OG complex, indicating that the hydration properties of the two detergents differ significantly and that the RC detergent belt contributes substantially to water sorption.

To analyze the sorption data we choose the Hailwood and Horrobin model,[56] which assumes that water sorption is governed by two sets of equilibria: (a) formation of hydrates between water and definite sites of the absorbing complex and (b) formation of an ideal solid solution of water in the complex. Accordingly, adsorption data have been fitted to the Hailwood and Horrobin equation[56]

$$h = h_0\left(\frac{K_1 r}{1 + K_1 r} + \frac{K_2 r}{1 - K_2 r}\right) \qquad (2)$$

where h represents the equilibrium water content of the film, h_0 and K_1 are constants, proportional to the number and activity of the hydration sites, respectively (process a), and K_2 is related to the water activity of the solid solution formed by water condensing at the surface of the complex (process b). Best fitting to eq 2 (continuous lines in Figure 2) yields the h_0, K_1, and K_2 values reported in Table 1 and allows one to resolve the contributions to the film hydration of water adsorbed at (strong) binding sites (process a) and at (weak) condensation sites (process b). These contributions are shown as dashed curves in Figure 2B. The h_0 value is significantly larger in RC−LDAO as compared to RC−OG films, indicating in the latter system a smaller number of strong binding sites. The activity of the strong binding sites (K_1) is about 5 times larger in the presence of LDAO. The different K_1 and h_0 values appear to be mainly responsible for the systematically larger total hydration observed in the RC−LDAO as compared to RC−OG films. Similar best-fitting values have been, in fact, obtained in the presence of LDAO and OG for the water activity K_2 of the solid solution. This finding is consistent with the notion that K_2 governs the progressive binding of water molecules at condensation sites to form a multilayer structure: most of this water population, therefore, does not interact directly with the detergent micelle which surrounds the RC.

3.2. Spectral Analysis of the Water Combination and Association Bands. The shape and location of the water combination band appear to be governed mostly by hydrogen-bonding organization.[46,57] This band can therefore provide information when attempting to qualify and quantify the intermolecular hydrogen bonds of water adsorbed to the RC−detergent complex. Upon decreasing r, particularly for r < 20%, the band as a whole shifted to lower wavenumbers and narrowed markedly (Figure 3). In RC−LDAO films the band peak shifted from 5160 cm^{-1} at r = 84% to 5000 cm^{-1} at 3%, and the bandwidth at the half-intensity

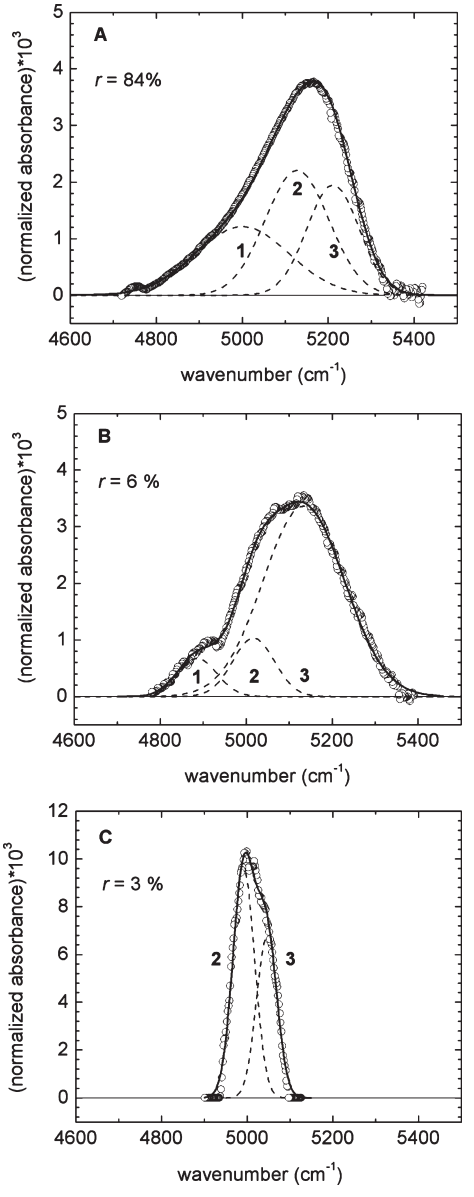

Figure 3. Resolution into three Gaussian components (dashed lines) of the combination band of water, corrected for the NH contribution (see Figure 1), in RC−LDAO films equilibrated at three different values of relative humidity: 84% (A), 6% (B), and 3% (C). Values of the fractional area, peak wavenumber, and width of the Gaussian components are reported in Figure 4.

decreased correspondingly from 245 to 100 cm^{-1}. Similar effects were observed in the RC−OG films.

In an attempt to resolve the contribution of water populations differing in structure and/or dynamics we performed a numerical

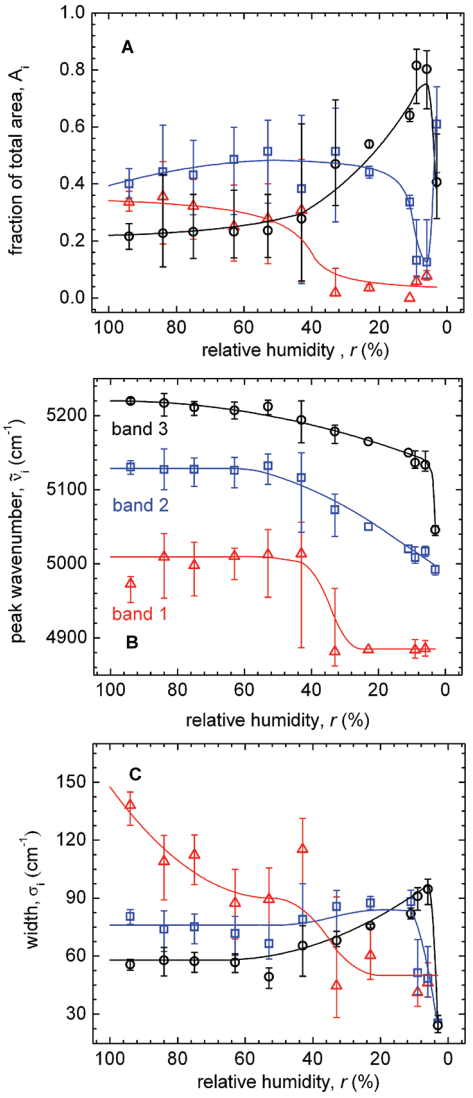

Figure 4. Fractional area (A), peak wavenumber (B), and width (C) of the three Gaussian components of the water combination band in RC−LDAO films as a function of the relative humidity, *r*. Bands are numbered according to the increasing value of their peak wavenumber as band 1 (red triangles), band 2 (blue squares), and band 3 (black circles). Vertical bars correspond to the confidence interval within 2 standard deviations of the parameters of the Gaussian components. Continuous lines are drawn through the experimental points just to guide the eye.

decomposition of the band into three Gaussian sub-bands. Such a decomposition has been previously employed to analyze the combination band of water in solution as a function of temperature[47,58,59] in mixed solvent systems,[45,57] and when adsorbed to solid surfaces.[60] The same Gaussian decomposition has been successfully applied to analyze the temperature dependence of the OH stretching band in pure water[61] and the effect of the water-to-detergent ratio on the OH stretching band in reverse micellar aggregates.[62] In all these systems the resolved bands are attributed to water subpopulations differing in the H-bonding organization. The lowest frequency Gaussian is assigned to molecules having a high H-bond coordination number, as this component sits close to the band observed in ice. Conversely, the highest frequency Gaussian is ascribed to water molecules poorly connected to their environment, according to the idea that the less H bonds are established the stiffer the oscillator.

After normalization of the bands to a unitary area, the absorbance A as a function of the wavenumber $\tilde{\nu}$ was fitted to

$$A(\tilde{\nu}) = \frac{1}{\sqrt{2\pi}} \sum_{i=1}^{3} \frac{A_i}{\sigma_i} \exp\left[-\frac{(\tilde{\nu} - \tilde{\nu}_i)^2}{2\sigma_i^2} \right] \quad (3)$$

with A_i, $\tilde{\nu}_i$, and σ_i as adjustable parameters. Examples of the obtained decomposition in RC−LDAO films are shown in Figure 3 for three values of *r*. Gaussian sub-bands are labeled as band 1−3 in order of increasing peak wavenumber. The dependence upon *r* of the best-fitting parameters, i.e., the fractional area (A_i), position ($\tilde{\nu}_i$), and width (σ_i) of the sub-bands, is presented in Figure 4 for RC−LDAO films. Under the most hydrating condition (r = 94%), the peak positions ($\tilde{\nu}_1$ = 4990 cm^{-1}, $\tilde{\nu}_2$ = 5125 cm^{-1}, $\tilde{\nu}_3$ = 5220 cm^{-1}) and widths (σ_1 = 140 cm^{-1}, σ_2 = 80 cm^{-1}, σ_3 = 55 cm^{-1}) of the three sub-bands essentially coincide with those found in pure water at a comparable temperature.[47,58,59] The band widths follow the order $\sigma_1 > \sigma_2 > \sigma_3$. This is consistent with the attribution of the lowest frequency band to water molecules for which the H-bonding connection is maximized, since hydrogen bonding is known to increase the breath of the band, in parallel with a decrease of the frequency.[63] In fully hydrated films, it appears therefore that the resolved subpopulations exhibit the spectral properties of pure water components, suggesting that most of the adsorbed water molecules are H bonded as bulk water and do not interact with the protein−detergent complex.

At values of the relative humidity between 94% and about 40% the sub-bands did not undergo significant changes, except for a slight shift to lower wavenumbers of bands 2 and 3 and a decrease of the width of band 1. At lower *r* values, however, dehydration of the film resulted in marked alterations, particularly prominent at r < 10%. The contribution of band 1 essentially vanished at r < 40%. The disappearance of band 1 was accompanied by a progressive increase of the fractional area of band 3, from about 0.25 at r = 40% to about 0.80 at r = 9%; this increase occurred also at the expenses of band 2. Further, extensive dehydration (from r = 6% to r = 3%) induced a sudden reduction of the contribution of band 3, compensated by the increase of band 2 fractional area. In parallel with these drastic changes, the peaks of bands 2 and 3 shifted to lower frequencies by about 150 cm^{-1}. Dehydration at r < 10% also induced a strong narrowing of bands 2 and 3.

In RC−OG films spectral analysis evidenced essentially a similar dependence upon *r* of the fractional area of the position and width of the three Gaussian sub-bands (not shown). In particular, in the hydrated RC−OG films (r = 94%) the peak positions and widths coincided within experimental error with those determined in the hydrated RC−LDAO films. Also, in the presence of OG, the fractional area of band 1, close to 0.3 at r = 94%, decreased upon dehydration and reduced to zero at r < 40%. This decrease occurred mainly at the expense of band 3, the contribution of which was maximum at r = 11%. The sudden increase of the fractional area of band 2, paralleled by a decrease of that of band 3, was also observed in RC−OG films at r < 9%. The shift to lower frequency of bands 2 and 3 was the same in RC−LDAO and RC−OG films. In the latter system these two bands underwent a larger narrowing ($\sigma_2 \cong \sigma_3 \cong$ 20 cm^{-1} at r = 3%).

The disappearance of the lowest frequency band 1 upon decreasing the hydration of the film below r = 40% appears to correlate with the strong decrease observed at this relative humidity in the amount of weakly adsorbed water, as resolved by

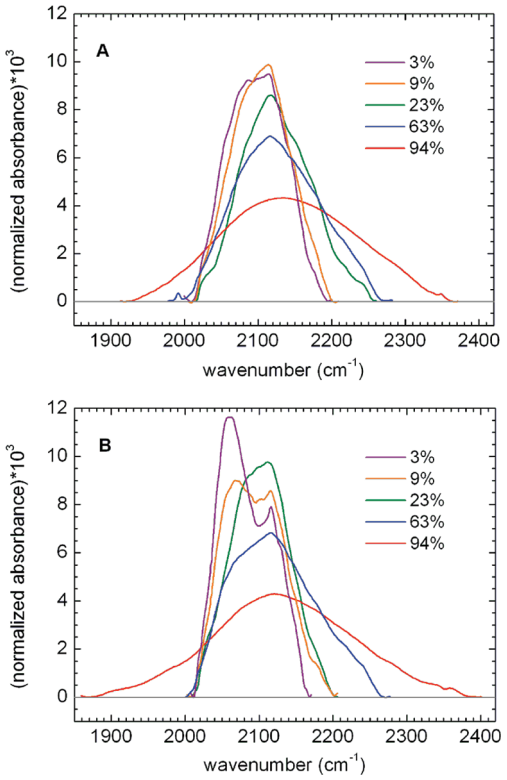

Figure 5. Evolution of the association band of water as a function of the relative humidity r in RC−LDAO (A) and RC−OG (B) films. The r values are indicated in the labels.

fitting the hydration isotherms to the Hailwood and Horrobin equation. As shown in Figure 2B, in fact, the contribution of this subpopulation of adsorbed water molecules, presumably condensed in multilayer structures, is strongly reduced upon decreasing the relative humidity from 94% to about 40%. Specifically, at $r <$ 45% in RC−LDAO films and $r <$ 30% in RC−OG films the contribution of the water adsorbed at strong binding sites starts to prevail over the weakly bound subpopulation. Consistently, band 1 is attributed to water molecules organized in structures highly connected through H bonding, which are characteristic of pure water.[47,58,59] The increase in the relative contribution of band 3 which accompanies the disappearance of band 1 and the decrease of band 2 (see above) is paralleled by a downward shift of their peak wavenumber at r values decreasing from ∼40% to ∼10%. This response, indicative of a strengthening of the H bonds involving these two water populations, suggests that water molecules adsorbed at stronger binding sites of the protein−detergent complex are progressively depleted upon drying. When the films are drastically dried, at 10% > r > 3%, the steep variations observed in the relative area of bands 2 and 3, the additional downward shift of the peak wavenumber, and the strong narrowing of both sub-bands indicate that drastic changes occur in the structure/dynamics of the residual water when the inner hydration shell is removed.

Additional information to characterize the interaction between water and the RC−detergent complex is provided by a second IR band of water, the so-called association band around 2130 cm^{-1}, ascribed to a combination of the bending mode of water with intermolecular vibrational modes.[64] The association band, which is absent in water vapors and is not structured in pure liquid water, becomes sizably structured when water interacts with phospholipids and acylglycerols in liquid-crystalline phases[65] and in powders of disaccharides,[66] suggesting that the coupling of the bending modes of water molecules with intermolecular modes involves also nonwater H-bonding groups.[67] This makes the band potentially useful when analyzing the structural organization of water adsorbed to RC−detergent films, since, at sufficiently low hydration levels, it can reflect the multiplicity of the environments experienced by the water molecules.

Figure 5A and 5B shows the association band of water measured in RC−LDAO and RC−OG films at selected values of the relative humidity; bands were normalized to a unitary area in order to better examine the evolution of the band in terms of width and structuredness. In the presence of both detergents the band underwent a progressive, strong narrowing but remained scarcely structured when dehydrating the film down to a relative humidity of about 10%. At lower r values no further narrowing occurred in the bands, which however became strongly structured. A pronounced shoulder appeared around 2080 cm^{-1} in the RC−LDAO film. In the RC−OG film a shoulder at approximately this wavenumber was already evident at r = 23%. At $r \leq$ 9% structuring of the band resulted in two well-resolved peaks at 2070 and 2120 cm^{-1}. In light of the arguments summarized above, this behavior suggests that when the RC−detergent films are equilibrated at $r <$ 10% the residual water interacts prevalently with surface groups of the protein and of the detergent micelle surrounding the hydrophobic portion of the RC. Consistently, the profile of the association band was very similar in highly hydrated RC−LDAO and RC−OG films (where water−water intermolecular modes mainly contribute to the association band), while on the contrary, it differed significantly in extensively dried films (where the fraction of weakly adsorbed water molecules, mostly interacting with other water molecules, is expected to be greatly reduced).

The area of the intramolecular $(\nu_2 + \nu_3)$ combination band of water is proportional to the total water content of the sample, being essentially independent of the extent of interaction of water with neighboring molecules (see above). At variance, the area of the association band, due to its intermolecular origin, strongly depends on the specific interaction of the water molecules with the environment, showing large differences between liquid water and ice.[68] This sensitivity was clearly shown by studies in which the ratio r_A between the area of the association (A_A) and of the combination (A_C) bands was determined in pure water, in water−sugar powders, and in protein−water−sugar glassy systems under different hydration conditions and in the presence of different saccharides.[67] When comparing pure water with trehalose dihydrate powders r_A was found to increase from 1.8 to 73. The value of r_A increased by at least one order of magnitude upon extensive dehydration of sugar−water−protein amorphous systems. Furthermore, the r_A value measured in the driest matrices depended significantly on the structure of the saccharide molecule. From these studies it was argued that the ratio r_A estimates roughly the extent of the interaction of water molecules with nonwater H-bond-forming groups, with large r_A values indicating large fractions of water molecules H bonded with nonwater groups.[67] The r_A values calculated from the area A_A and A_C measured in RC−LDAO and RC−OG films at different values of relative humidity are reported in Table 2. At 11% < r < 94%, the r_A ratio does not show systematic changes, fluctuating around an average value close to 0.9. At lower contents of residual water the r_A value increases, jumping to 36 and 50 in the driest (r = 3%)

Table 2. Ratio $r_A = A_A/A_C$ between the Area Underlying the Association (A_A) and Combination (A_B) Band of Water As a Function of the Relative Humidity r Determined in RC−LDAO and RC−OG Films

r (%)	94	84	75	63	53	43	33	23	11	9	6	3
r_A (RC−LDAO)	1.20	0.88	0.78	0.86	0.74	0.64	0.84	0.88	0.77	1.37	1.80	36.4
r_A (RC−OG)	1.43	0.98	1.30	0.80	0.80	0.84	0.81	0.85	1.01	2.02	1.69	50.1

RC−LDAO and RC−OG films, respectively. This behavior is in line with the one observed in protein−water−sugar glassy systems[67] and suggests that under the driest conditions the large majority of the adsorbed water molecules interact directly with nonwater H-bonding groups of the RC−detergent complex.

3.3. Recombination Kinetics of the Primary Charge-Separated State $P^+Q_A^-$. As outlined in the previous paragraphs, the thermodynamic and spectral analyses of water sorption by RC−detergent films concur to identify two main hydration regimes. When the relative humidity is decreased from 94% to about 30% the amount of adsorbed water undergoes a large change from 35×10^3 to 1.6×10^3 H_2O molecules per RC in RC−LDAO films and from 8×10^3 to 6×10^2 H_2O molecules per RC in RC−OG films (Figure 2). At $r > 30\%$, the combination band of water exhibits spectral features similar to those of bulk water (Figure 4), indicating that such a change of the relative humidity affects essentially the number of water molecules weakly bound at condensation sites (Figure 2). However, the progressive narrowing of the intermolecular association band observable over this hydration range (Figure 5) suggests that depletion of the outer hydration shell already affects the structural organization and dynamics of the residual water. Such changes are reflected also in the intramolecular water combination band (Figure 4) only when (at $10\% < r < 30\%$) the amount of bound water is further reduced to $\sim 10^3$ and ~400 H_2O molecules per RC in RC−LDAO and RC−OG films, respectively. Hydration isotherms show indeed that under these conditions the contribution of water adsorbed to strong binding sites of the complex becomes relevant and overcomes the contribution of the weakly bound water molecules. Finally, dramatic changes are observed both in the combination and in the association band when the second hydration regime is entered, at $r < 10\%$, i.e., when the most tightly bound water molecules, presumably forming the inner hydration shell, are removed progressively.

In order to examine how the extent of hydration and the structure/dynamics of the hydration shell affect intraprotein electron transfer we analyzed the kinetics of flash-induced $P^+Q_A^-$ recombination in RC−detergent films as a function of their water content. Kinetic measurements were performed in parallel with the spectral analysis described above over the same samples.

As summarized in the Introduction the recombination kinetics of the light-induced $P^+Q_A^-$ state can be considered a sensitive probe of (a) the RC relaxation from the dark-adapted to the light-adapted conformation in response to the electric field generated by the light-induced charge separation and (b) the RC thermal fluctuations among a large ensemble of conformational substates. In room-temperature RC solutions both processes occur rapidly over the time scale of the electron transfer reaction, so that an almost exponential recombination kinetics is observed from the light-adapted, stabilized conformation of the $P^+Q_A^-$ state. When relaxation from the dark- to the light-adapted conformation is hampered (e.g., at cryogenic temperatures in water−glycerol systems[5,13] or at room temperatures when the RC is incorporated into dehydrated sugar glasses[33,36,37] or polymeric matrices[37,69]) $P^+Q_A^-$ recombination is accelerated significantly. Under these conditions, the kinetics becomes markedly nonexponential, being described by a continuous distribution of rate constants: the broadening of the rate distribution is taken to indicate a drastic slowing of the interconvesion among RC conformational substates.[5,33] Analysis of $P^+Q_A^-$ recombination in RC−detergent films characterized by a different, controlled hydration is therefore expected to provide information on the conformational dynamics of the RC and on its coupling with the structure and dynamics of the RC−detergent hydration shell.

Figure 6A shows the kinetics of $P^+Q_A^-$ recombination measured by recording the absorbance change at 422 nm after a laser pulse in RC−LDAO films equilibrated at relative humidity between 63% and 9%. Dehydration of the RC−detergent complex results in a progressive acceleration of the kinetics, which become also more and more distributed. A similar behavior was observed in RC−OG films (see below). To account for the nonexponential, distributed character of the kinetics, we fitted the time dependence of the $P^+Q_A^-$ survival probability, $N(t)$, to a power law[70]

$$N(t) = \frac{\Delta A_{422}(t)}{\Delta A_{422}(0)} = (1 + k_0 t)^{-n} \quad (4)$$

where $\Delta A_{422}(t)$ is the absorbance change at time t, $t = 0$ is the time of the laser pulse, and k_0 and n are free parameters. This parametrization, first adopted to analyze $P^+Q_A^-$ recombination in RC frozen at cryogenic temperature,[13] has been largely used to fit the kinetics measured in RCs embedded in dried amorphous matrices.[33,36,37] The choice of a power law has the advantage of providing an analytical form for the rate distribution $p(k)$ which describes the kinetics according to

$$N(t) = \int_0^\infty p(k) e^{-kt}\, dk \quad (5)$$

In fact, the inverse Laplace transform of $N(t)$, takes the form of a Gamma distribution

$$p(k) = L^{-1}[N(t)] = \frac{k^{n-1} \exp(-k/k_0)}{k_0^n \Gamma(n)} \quad (6)$$

where $\Gamma(n)$ is the Gamma function and the parameters k_0 and n are related to the average rate constant, $\langle k \rangle$, and to the variance, σ^2, of the rate distribution by

$$\langle k \rangle = nk_0 \quad \sigma^2 = nk_0^2 \quad (7)$$

Fitting to eq 4 yielded a reasonable description of the kinetics measured in RC films equilibrated at relative humidity r as low as 23% (see Figure 6A and 6B). In hydrated films, characterized by ~4300 H_2O molecules per RC ($r = 63\%$), $\langle k \rangle = 15.3 \pm 0.2$ s^{-1}. Upon dehydration $\langle k \rangle$ increases and reaches a value of 27.8 ± 0.6 s^{-1} when the hydration layer is decreased to ~1400 H_2O molecules per RC ($r = 23\%$). As shown in Figure 6C, the acceleration of the kinetics is paralleled by a progressive broadening of the rate distribution. To allow a more direct comparison with the rate distributions obtained at low temperatures[5] or in

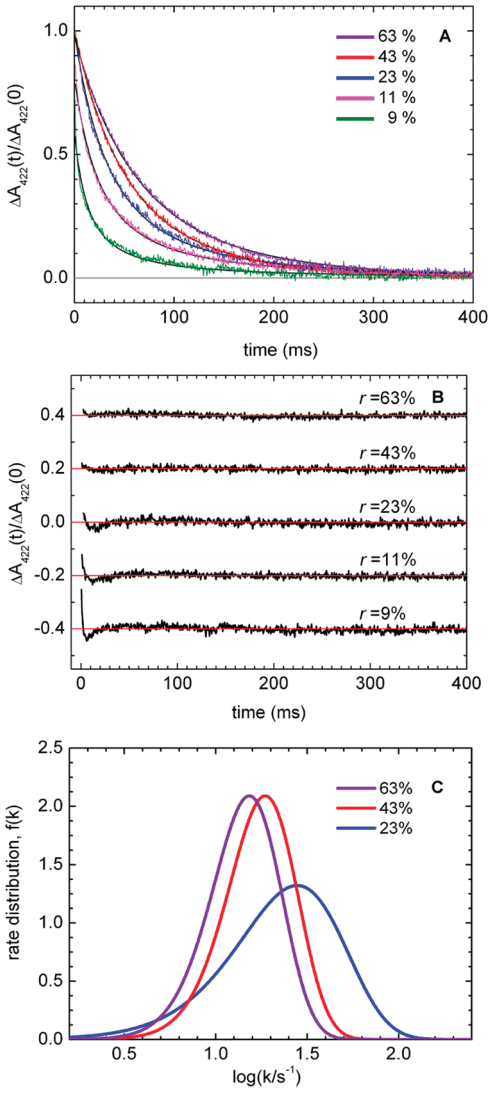

Figure 6. Kinetic analysis of $P^+Q_A^-$ recombination following laser flash excitation of RC−LDAO films equilibrated at the indicated relative humidity *r*. (A) Normalized decay of the $P^+Q_A^-$ state. Best fits to eq 4 are shown as black continuous lines. The values of the average rate constant $\langle k \rangle$ and distribution width σ are reported in the following only for the kinetic traces measured at $r \geq 23\%$, i.e., for the kinetics which satisfactorily fit a power law (see panel B). The extremes of the calculated confidence intervals within two standard deviations are indicated in brackets. Fit to eq 4 yielded the following: $\langle k \rangle$ = 15.3 (15.1, 15.5) s^{-1}, σ = 6.6 (6.3, 6.9) s^{-1} at *r* = 63%; $\langle k \rangle$ = 18.6 (18.4, 18.9) s^{-1}, σ = 8.1 (7.7, 8.4) s^{-1} at *r* = 43%; $\langle k \rangle$ = 27.8 (27.2, 28.5) s^{-1}, σ = 18.6 (17.9, 19.4) s^{-1} at *r* = 23%. Although for the sake of visual clarity only the first 400 ms of $P^+Q_A^-$ decay are shown, the time scale of kinetic recording (time resolution 0.5 ms) extended out to 1 s after the laser pulse and the whole information was used when fitting kinetics to eq 4. (B) Residues of the fit to eq 4. Traces have been arbitrarily shifted along the vertical scale. (C) Rate distributions $f(k)$ corresponding to the fit to a power law of the kinetics at *r* = 63%, 43%, and 23%. The distributions, calculated according to eq 6, are defined on a logarithmic scale.

dehydrated matrices[33,36] we show rate distributions $f(k)$ defined on a logarithmic *k* scale ($f(k)\mathrm{d}\log(k) = p(k)\mathrm{d}k$). From the described kinetic effects (Figure 6) we infer that dehydration of the film progressively hampers the RC relaxation from the dark-adapted to the light-adapted conformation and concomitantly

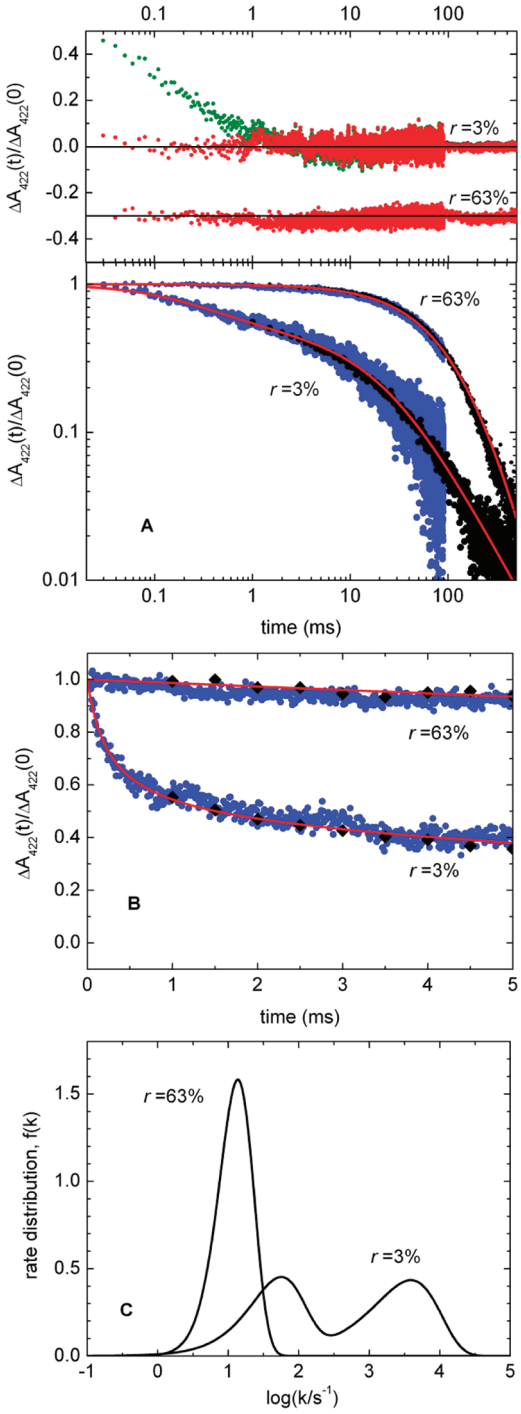

Figure 7. Kinetic analysis of $P^+Q_A^-$ decay in RC−LDAO films equilibrated at relative humidity *r* = 63% and 3%. Data have been acquired on each sample in two sets with time resolutions of 10 μs per point (blue trace) and 0.5 ms per point (black trace). Data recorded over both time windows were used when fitting the kinetics. (A) Log−log plot of the normalized kinetics. The best fit to a single power law (eq 4) at *r* = 63% and to the sum of two power laws (eq 8) at *r* = 3% are shown as continuous red lines. (Top) Corresponding residues (red dots) and residues of the fit to a single power law (eq 4) for the kinetic trace at *r* = 3% (green dots). (B) Expanded view of the first 5 ms of the decays. (C) Rate distribution functions $f(k)$, defined on a logarithmic scale, calculated according to eqs 6 (at *r* = 63%) and 9 (at *r* = 3%) from the best-fitting parameters.

dx.doi.org/10.1021/jp2057767 |J. Phys. Chem. B 2011, 115, 14732–14750

inhibits the RC thermal fluctuations. Both dynamics are affected by a reduction of the weakly bound hydration layer, since a decrease of r from 63% to 23% mainly affects this subpopulation of the adsorbed water, without depleting the tightly bound water layer (Figure 2).

When the hydration of the RC−LDAO film is further reduced (at r < 23%) the recombination kinetics is further accelerated (Figure 6A). Under such dehydrated conditions eq 4 becomes unable to fit adequately the kinetics: as shown in Figure 6B, in fact, while in hydrated samples the residues of the fit to eq 4 are randomly distributed, for traces acquired at r < 23% the residues exhibit a systematic increase at short times after the laser, suggesting the presence of an additional, faster kinetic component which cannot be accounted for by eq 4. This unsatisfactory residue pattern, which already appears in the trace at r = 23%, becomes more and more evident upon dehydration, when r is decreased from 11% to 9% (Figure 6B). In order to better analyze the short time behavior we increased the time resolution of the kinetic measurements to 10 μs over the 0−100 ms time range. Figure 7 shows an example of the kinetics measured at higher time resolution under extremely dehydrated conditions (r = 3%) as compared to the kinetics measured in the hydrated film (r = 63%). The log−log plot of Figure 7A (lower panel) makes evident that at variance with the trace at r = 63% under the most dehydrated conditions the decay is drastically distributed in rate, occurring over more than 4 orders of magnitude. Figure 7A and 7B suggests that the faster kinetic component present at r = 3% is also markedly distributed in rate. We found that kinetic traces acquired at r < 23% fit well the sum of two power laws, i.e.

$$N(t) = (1 - A_f)(1 + k_0 t)^{-n} + A_f(1 + k_{0f} t)^{-n_f} \qquad (8)$$

where A_f is the relative amplitude and k_{0f} and n_f are the kinetic parameters of the fast phase. The best fit to a single power law (eq 4) of the kinetics at r = 63% and to the sum of two power laws (eq 8) for the kinetics measured at r = 3% is shown as red lines in Figure 7A (lower panel) over the whole time window examined and in Figure 7B over a time scale which better resolves the fast phase at r = 3%. The inability of a single power law (eq 4) to fit the kinetics in strongly dehydrated RC−detergent films, already suggested by the residue distribution of the traces acquired at the lower time resolution (Figure 6B), is seen more clearly at the higher time resolution. As illustrated in the upper panel of Figure 7A, the residues of the fit to a single power law (eq 4) are uniformly distributed in the hydrated sample (r = 63%) but increase systematically in the most dehydrated RC−detergent film (r = 3%) at short times (green dots). In the upper panel of Figure 7A, the residues of this unacceptable fit are compared with those of the fit to the sum of two power laws (eq 8), which at variance appear randomly distributed also in the short time range (see red dots, r = 3%). Similar patterns of residues were obtained when comparing the best fit to eqs 4 and 8 in all kinetic traces measured at higher time resolution for r < 23% in the presence of the both detergent LDAO and OG. Consistently, the fit to the sum of two power laws (eq 8) yielded *reduced* chi-square values systematically lower than the fit to a single power law (eq 4) at r < 23%. As a possible alternative to eq 8 and to further test the presence of a second kinetic component under strongly dehydrated conditions, we fitted the kinetics also to a stretched exponential, i.e., to the Kohlrausch−Williams−Watts (KWW) decay function $N(t) = \exp[-(t/\tau)^{\beta}]$, with τ and β as free parameters. The KWW function, although providing a fit better than eq 4 in strongly

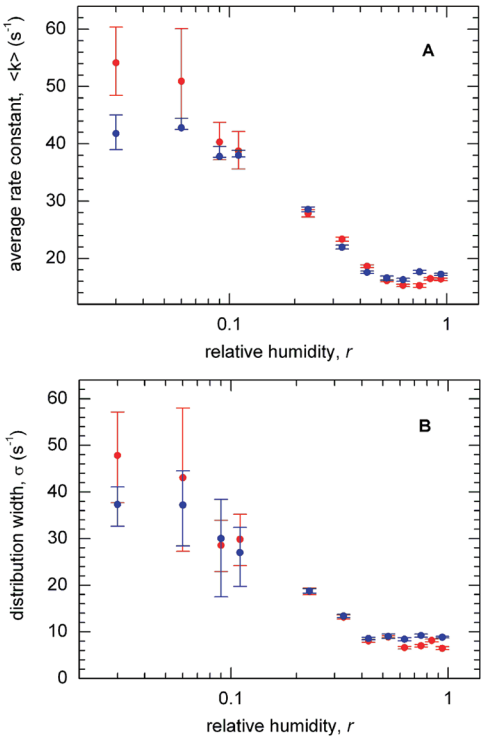

Figure 8. Dependence of the kinetics of $P^+Q_A^-$ recombination upon the relative humidity, r, in RC−LDAO (red circles) and RC−OG (blue circles) films. (A and B) Values of the average rate constant $\langle k \rangle$ and rate distribution width σ, respectively. Kinetic analysis was performed as described in the text and illustrated in Figures 6 and 7. When the $P^+Q_A^-$ decay includes two kinetic phases, i.e., in films equilibrated at r < 23%, the plotted $\langle k \rangle$ and σ values refer to the slow phase. The corresponding kinetic parameters of the fast phase are reported in Table 3. Vertical bars indicate confidence intervals within two standard deviations.

dehydrated RC−detergent films, yielded reduced chi-square values slightly but systematically larger than the fit to the sum of two power laws (eq 8). Furthermore, the residues of the best fit to the KWW function exhibited a significant and systematic increase in the 0−1 ms time range (not shown), indicating that the KWW function was not able to satisfactorily account for the short time behavior of the kinetics. This finding further supports the notion that an additional, distributed kinetic component appears in the $P^+Q_A^-$ decay upon extensive dehydration.

Use of eq 8 to describe the kinetics leads to a bimodal rate distribution function $p(k)$ given by the weighted sum of two Gamma distributions

$$p(k) = (1 - A_f)\frac{k^{n-1}\exp(-k/k_0)}{k_0^n \Gamma(n)} + A_f\frac{k^{n_f-1}\exp(-k/k_{0f})}{k_{0f}^{n_f}\Gamma(n_f)} \qquad (9)$$

The average rate constant $\langle k_f \rangle$ and the distribution width σ_f of the fast kinetic component are obtained from the fitting parameters k_{0f} and n_f through eq 7. The unimodal (eq 6) and bimodal (eq 9) rate distribution functions which describe the kinetics at r = 63% and 3%, respectively, are represented in Figure 7C.

The values of $\langle k \rangle$ and σ obtained for the slow kinetic component are plotted in Figure 8 as a function of the relative humidity r at which the film was equilibrated. The kinetic parameters of the

Table 3. Kinetic Parameters of the Fast Phase of $P^+Q_A^-$ Recombination Detected upon Extreme Dehydration of RC−LDAO and RC−OG Films[a]

relative humidity, r (%)	H_2O/RC molar ratio	relative amplitude, A_f (%)	average rate constant, $\langle k_f \rangle$ (s^{-1})	distribution width, σ_f (s^{-1})
		RC−LDAO		
11	935	38.9 (33.0, 45.8)	1569 (568, 3964)	1505 (398, 5458)
9	815	61.0 (54.1, 69.2)	3421 (2537, 4622)	3660 (2152, 8332)
6	670	60.2 (55.3, 65.8)	3668 (2547, 6004)	4136 (2729, 7370)
3	85	56.4 (50.5, 63.3)	3884 (2882, 5658)	4211 (2754, 8164)
		RC−OG		
11	435	47.1 (42.4, 52.4)	1678 (1412, 2021)	1805 (1501, 2203)
9	330	61.4 (55.8, 68.2)	1780 (1540, 2083)	1908 (1625, 2238)
6	305	55.9 (51.9, 60.5)	1913 (1614, 2312)	2114 (1816, 2552)
3	30	42.0 (37.5, 46.5)	1705 (1447, 2032)	2223 (1893, 2648)

[a] The extremes of the calculated confidence intervals within two standard deviations are indicated in brackets.

fast component are reported in Table 3. In both RC−LDAO and RC−OG films the fast kinetic phase appears abruptly when the films are equilibrated at $r < 23\%$: its relative amplitude exceeds 50% of the total at $r = 9\%$ and remains unaffected within experimental error when the residual water of the films is further reduced. Also, the average rate constant $\langle k_f \rangle$ and distribution width σ_f of the fast component stay essentially constant at $3\% \leq r \leq 9\%$, around 3.5×10^3 and 1.8×10^3 s^{-1} in RC−LDAO and RC−OG films, respectively.

Quite remarkably, although the water content of the RC−LDAO and RC−OG films differs considerably at each value of r (see Figure 2), Figure 8 shows a single dependence of $\langle k \rangle$ and σ upon the relative humidity, irrespective of the chemical nature of the detergent. The simplest interpretation of this behavior appears to be that the hydration of the detergent belt has a negligible impact on the RC dynamics probed by the kinetics of charge recombination (see Discussion). The increase of $\langle k \rangle$ and σ occurs steeply below a threshold value of relative humidity $r \approx 0.4$ This value of r corresponds to a molar ratio H_2O/RC of ∼2000 and ∼1000 in the presence of LDAO and OG, respectively. When the fast kinetic component becomes detectable at $r \approx 0.1$, corresponding to H_2O/RC ≅ 900 in RC−LDAO and H_2O/RC ≅ 400 in RC−OG films, both $\langle k \rangle$ and σ have already increased by almost three times and appear to be close to their maximal values reached at the minimum value of the relative humidity. The continuity found in the values of $\langle k \rangle$ and σ over the whole range of relative humidity, even when a second additional kinetic phase, characterized by $\langle k_f \rangle$ and σ_f, has to be included in the fit, supports the physical adequacy of the fitting model adopted in the kinetic analysis. Interestingly, the fast kinetic component of P^+ decay is observed rather abruptly when all the weakly bound water molecules have been essentially withdrawn and a significant fraction of the inner most tightly bound hydration shell has been also removed, as judged from the water sorption isotherms (cf. Figure 2B).

The fast phase of the decay measured at 422 nm occurs on the hundreds of microseconds time scale (Figure 7 and Table 3). To attribute safely this kinetic component to $P^+Q_A^-$ recombination, excluding side electron donation which could concur to rereduce P^+ and reoxidize Q_A^-, we measured in parallel the decay of the laser-induced absorbance change at 450 nm, i.e., at the peak of the differential semiquinone/quinone spectrum. As detailed in section 2.2, at 422 nm the relative contribution of P^+ to the flash-induced absorbance change largely dominates. At 450 nm the contribution of Q^- becomes more significant (∼40%). If events different from $P^+Q_A^-$ recombination contribute to the decay of the photogenerated radical pair we expect that the kinetics of P^+ and Q_A^- recovery after photoexcitation will in general differ, resulting in a different kinetics of the absorbance change measured at 422 and 450 nm. The time course of signals recorded in parallel at 422 and 450 nm was always found to coincide, even in RC−detergent films equilibrated at $r = 3\%$ (not shown). This observation strongly supports the attribution to $P^+Q_A^-$ recombination of both kinetic phases measured under the most dehydrating conditions. Thus, under extreme dehydration two RC populations can be identified in which the stability of the primary charge-separated state differs by almost 2 orders of magnitude.

4. DISCUSSION

4.1. Hydration Shell of the RC−Detergent Complex: Thermodynamic Properties and Structural Organization. Water sorption by RC−detergent complexes can be studied profitably by coupling the use of thin films of the protein−detergent complex with the isopiestic method to control hydration. The combination band of water at 5155 cm^{-1} is well suited to study water binding to protein complexes: its position and width yield information on the H-bonding organization of water molecules, while the area below the band measures the amount of bound water, being independent of the H-bonding organization.[45−47] The sensitivity of the FTIR spectroscopic determination of water makes possible the study of water sorption/desorption on small amounts of RC−detergent complexes (about 1 mg) which equilibrate rapidly (typically in a few hours) at a relative humidity between 94% and 3%.

Hysteresis phenomena have been reported in several investigations involving desorption/sorption cycles on soluble proteins (see, e.g. ref 55). Scanning experiments on α-chymotripsin and tropocollagen have shown however that hysteresis effects occur only as a consequence of an almost complete water removal.[55] Our data (section 3.1) do not reveal any hysteresis effect. We could, for instance, verify that the water content of a film equilibrated at $r = 63\%$ was independent of its dehydration/rehydration history, i.e., the same for the following desorption/sorption sequences: (i) solution → ($r = 63\%$); (ii) solution → ($r = 11\%$) → ($r = 63\%$); (iii) solution → ($r = 3\%$) → ($r = 6\%$) → ($r = 9\%$) → ($r = 63\%$). We consider this as a reasonable test that the obtained

data represent true equilibrium states, accessible to thermodynamic interpretation.

The sorption isotherms obtained in RC−LDAO and RC−OG films (Figure 2) exhibit the typical sigmoidal type II character[71] observed for a large number of polypeptides. To describe such a behavior different theoretical models, roughly falling in two classes (surface and solution models), have been adopted (for a review, see ref 72). Our data fit well the Hailwood and Horrobin equation (eq 2), based on a solution model, which provides a convenient way to separate the "monolayer" (tightly bound water) and "multilayer" (weakly bound water) contributions to a given isotherm. The equation includes only three adjustable parameters, related to the number (h_0) and activity (K_1) of "tight" binding sites ("monolayer" component) and to the activity (K_2) of water condensing in "multilayer" structures. We also fitted our experimental isotherms to the D'Arcy and Watt equation,[73] which accounts for an additional set of weak binding sites. Although an equally good fit was obtained (not shown), confidence analysis resulted in unacceptably large uncertainties of the parameters, indicating that no information was gained and that the Hailwood and Horrobin equation yielded a possibly rough but physically more sound interpretation of the data.

At any value of relative humidity the H_2O/RC molar ratio is approximately two times larger in RC−LDAO as compared to RC−OG complexes, indicating that the binding of water to the detergent belt which surrounds the hydrophobic region of the RC contributes substantially to the overall water sorption process. The best-fitting parameters (Table 1) show that the activity K_2 of water in the solid solution is comparable for RC−LDAO and RC−OG complexes, as expected for water molecules which form the outermost hydration shells. The larger hydration systematically observed in RC−LDAO as compared to RC−OG is traced back to the larger number h_0 of binding sites and to the ∼5 times larger activity K_1 of water forming the inner hydration layer. Since both the exposed hydrophilic portion of the RC protein and the surface of the detergent belt are expected to bind water molecules, we discuss in the following a simple geometrical model of the RC−detergent complex, which allows a rough estimate of the water binding surfaces in the case of LDAO and OG solubilized RCs.

The number of LDAO molecules associated with the RC from *Rb. sphaeroides* (wild-type Y) has been determined by chromatography using ^{14}C-labeled detergent. Values of 206 ± 12[74] and 289[75] have been reported. By monitoring the resolubilization of detergent-free RC preparations from *Rb. sphaeroides* R26 values of 150 ± 20 and 370 ± 100 were obtained at pH 8.0 for LDAO and OG, respectively.[76] Using LDAO/RC = 150 or 289 and OG/RC = 370 ± 100 it can be easily evaluated that in the solutions used to prepare our RC−detergent films (0.025% LDAO or 0.1% OG) the molar ratio ("free"/total) detergent is about 11% or 6% (LDAO) and (13 ± 3)% (OG); we assume therefore that in our samples essentially all the detergent is associated with the RC protein. The low-resolution structure of the RC−detergent complexes obtained by neutron diffraction in crystals of *Rps. viridis* showed that LDAO is concentrated in rings, forming a micelle around the transmembrane helices of the RC.[77] The extension of this approach to localize the detergent OG in crystals of *Rb. sphaeroides* strain Y[78] indicated a quasi identity of the shape and position of the OG and LDAO rings around the transmembrane helices. In both cases the thickness of the detergent phase perpendicular to the membrane plane was nearly 30 Å, suggesting that the detergent belt can be regarded as a half-torus of

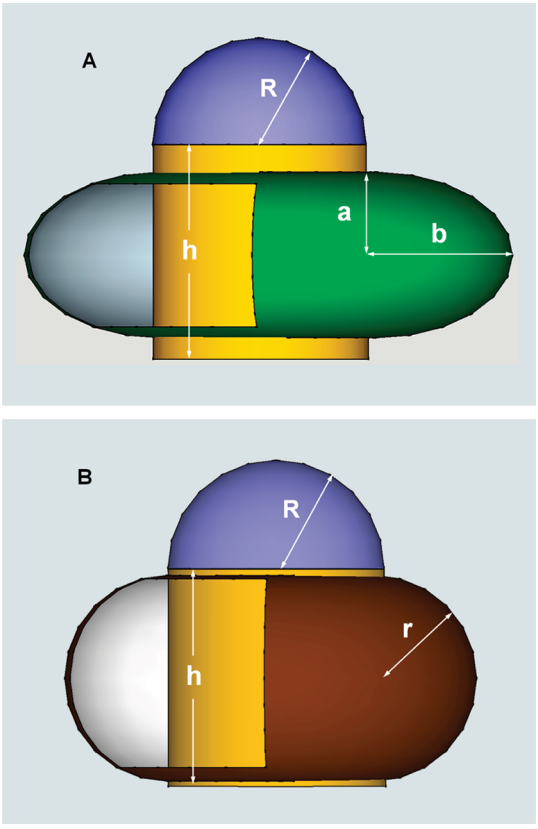

Figure 9. Geometrical model of the RC−LDAO (A) and RC−OG (B) complexes (see section 4.1 for details).

minor radius close to 15 Å. It has to be noted, however, that crystallization in the presence of LDAO can be accomplished only in conjunction with additional amphiphiles, such as 1,2,3-heptanetriol, which was present in the *Rps. viridis* crystals used to obtain the low-resolution structure of RC−LDAO complexes.[77] The micellar radius of LDAO in solution is significantly decreased upon addition of heptanetriol.[79] A SANS determination of micelle structure[80] has shown that addition of heptanetriol perturbs substantially not only the dimension but also the shape of pure LDAO micelles in solution. Thiyagarajan and Tiede[80] found that the LDAO micelle can be assimilated to an ellipsoid with semiaxes of 30.6 and 19.4 Å and the OG micelle to a sphere of radius 22.9 Å. Addition of heptanetriol to pure LDAO micelles resulted in smaller, spherical micelles with radii in the range 17−21 Å, in agreement with ref 79. In view of these results we believe that under the condition of our samples the shape and dimension of the detergent belt can be reasonably described using the parameters determined by Thiyagarajan and Tiede[80] for LDAO and OG micelles. Figure 9 shows the geometrical model we adopted. In a crude approximation subunits L and M of the RC have been represented as forming a cylinder of height h = 50 Å and radius R = 25 Å; the H subunit is approximated to a hemisphere of radius R, which caps the LM cylinder.[81] The LDAO belt (Figure 9A) is modeled as an oblate ellipsoidal ring, generated by rotation of half an ellipse of semiaxes a = 19.4 Å and b = 30.6 Å[80] removed by the distance R from the axis (of rotation) of the LM cylinder. We note that the choice of an oblate ellipsoidal ring implies a thickness of the detergent phase perpendicular to the membrane plane equal to $2a$ = 38.8 Å, in good

Table 4. Thermodynamic and Structural Parameters Used To Evaluate the Average Area A_{bp} Per Tightly Bound Water Molecule in Soluble Proteins[a]

protein	molecular weight (KDa)	pdb file	h_0 (g water/g protein)	h_0 (H_2O/protein) molar ratio	protein surface area (Å^2)	area per water binding site (Å^2)
lysozyme	14.331	2LYZ	0.080	64	5672	88.6
β-lactoglobulin	18.387	2Q2M	0.059	60	7881	131
α-chymotrypsin	25.000	3NK8	0.069	96	8102	84.4
ovalbumin	172.438	1OVA	0.058	556	57877	104.1

[a] The values of h_0, obtained by fitting the experimental sorption isotherms to the Hailwood and Horrobin equation, are from ref 55.

agreement with a calculated thickness of the hydrophobic portion of the RC LM subunit of 42 Å.[81] The OG belt (Figure 9B) is represented as a half torus of minor radius r = 22.9 Å, corresponding to the radius of the spherical OG micelle,[80] and major radius R. The surface area A_{HT} of the half torus is given by[82]

$$A_{HT} = 2\pi^2 rR + 4\pi r^2 \quad (10)$$

The surface area A_{OE} of the oblate ellipsoidal ring can be calculated as (see Appendix)

$$A_{OE} = \frac{2\pi b}{a}\int_{-a}^{+a}\left[a^2 - \frac{x^2}{a^2}(a^2 - b^2)\right]^{1/2} dx + 2\pi R\int_{-a}^{+a}\left[1 + \frac{b^2x^2}{a^2(a^2 - x^2)}\right]^{1/2} dx \quad (11)$$

by numerical integration. Starting from the geometrical model of Figure 9 and using eqs 10 and 11 it can be estimated that the area of the LDAO detergent belt is equal to 21.5 × 10^3 Å^2 while that of the OG ring is 17.9 × 10^3 Å^2. Unfortunately the large uncertainty in the number of detergent molecules per RC complex (see above) does not allow a strict test of consistency of the geometrical model with the surface area of the detergent head groups. However, the calculated area of the detergent LDAO and OG rings, when divided by the number n of detergent molecules per RC complex experimentally estimated, yields an area per LDAO molecule equal to 74 (for n = 289) or 143 Å^2 (for n = 150) and an area per OG headgroup equal to 48 ± 13 Å^2 (n = 370 ± 100). These values are reasonably consistent with literature data: a value of 44 Å^2 has been determined for the area of the headgroup of OG using independent experimental approaches;[65,83] for the LDAO headgroup, areas around 60 and 70 Å^2 have been determined by SANS, respectively, excluding or including hydration water. A recent molecular dynamics simulation of LDAO micelles[84] has provided a value of 94.8 Å^2, which compares favorably with the range derived from the area of the LDAO ring in our model.

In the geometrical model of Figure 9 the area of the exposed protein surface, not screened by the detergent ring, is equal to 7.65 × 10^3 (RC−LDAO) and 6.55 × 10^3 Å^2 (RC−OG), implying that the contribution of the protein surface interacting directly with water is ∼27% of the total surface area of the RC−detergent complex for both detergents. The total surface area is larger in RC−LDAO (29.2 × 10^3 Å^2) as compared to RC−OG complexes (24.4 × 10^3 Å^2). From these values and from the number h_0 of water binding sites derived from sorption isotherms (Table 1) we can estimate the average area per binding site, A_b, equal to 19.5 and 24.4 Å^2 for the RC−LDAO and RC−OG complex, respectively. A_b can be usefully compared with the average area per binding site estimated in soluble proteins. To this end, among the large number of available data, we selected those obtained in proteins for which Hailwood and Horrobin analyses of hydration isotherms and high-resolution crystallographic structures are available. The protein surface area accessible to water has been evaluated from the structural data (pdb files are listed in Table 4) using the "rolling ball" algorithm implemented in the Swiss-PdbViewer molecular graphics software with a radius equal to 1.4 Å. From the values of h_0 (g of water/g of protein)[55] and the evaluated surface area of the protein the area per water binding site has been calculated. The results, summarized in Table 4, indicate that the area per water binding site does not change too much over a set of structurally different proteins which span a large range of molecular masses, yielding an average area per binding site, A_{bp} = (102 ± 21) Å^2. This value is about 4−5 times larger than the average area per binding site A_b estimated over the whole RC−detergent complex. It appears therefore that the surface density of water molecules tightly bound to the detergent ring of the RC is much higher than the average density of water tightly bound to the protein surface. If we assume that the A_{bp} value evaluated from the data of Table 4 holds also for the exposed surface of the RC protein, the average area A_{bd} per binding site on the detergent belt can be evaluated from the relation

$$\frac{1}{A_b} = \frac{1}{A_{bp}}\left(\frac{A_p}{A_T}\right) + \frac{1}{A_{bd}}\left(\frac{A_d}{A_T}\right) \quad (12)$$

where A_p and A_d are the surface areas of the water-exposed RC protein and of the detergent ring, respectively, and $A_T = A_p + A_d$. From eq 12 we obtain A_{bd} =15 and 19 A^2 for LDAO and OG, respectively. These values, when considering the area per detergent headgroup evaluated from our geometrical model, would correspond to a number of water molecules tightly bound to each detergent head group ranging from ∼9 to ∼5 for LDAO and ∼2.5 for OG. The larger hydration of LDAO is in qualitative agreement with molecular dynamics simulations performed in LDAO[84] and OG[85] micelles, which resulted in an average hydration number ∼8 and ∼5, respectively.

According to the Hailwood and Horrobin fit, the activity K_1 of the strong water binding sites is about 5 times larger in the RC−LDAO as compared to the RC−OG complex (Table 1). Since the area of the exposed protein surface represents a comparable fraction of the total area in the RC−LDAO and RC−OG complexes, the observed difference in K_1 values implies that the water activity of the tight binding sites is even more than 5 times larger for the LDAO than for the OG molecules of the detergent ring which surrounds the RC. This observation is consistent with the H-bonding properties of the polar head of the two detergents, emerging from simulative studies. Amine oxides are highly hydrophilic despite having only one polar atom (oxygen) able to

interact with water. A recent ab initio study of the LDAO interaction with water[86] features a maximum of 3 water molecules H bonded to the amine oxide group. The mean energies of the H bonds (55, 52, and 49 kJ/mol for 1, 2, and 3 water molecules) are much larger than the H-bond energy of the water dimer (~13 kJ/mol[87,88]). As to the strength of the H bonds between the OG hydroxyl groups and water, ab initio molecular dynamics simulations of a glucose−water system indicate that hydroxyl groups form weak acceptor and stronger donor H bonds.[89] The strength of the latter was found comparable to that of the water dimer.

Finally, we notice that a description of water sorption to soluble proteins (lysozyme, β-lactoglobulin, α-chymotrypsin, ovalbumin) according to the Hailwood and Horrobin isotherm[55] yielded K_1 values between ~9 and ~15, which are comparable to the K_1 value determined for the RC−LDAO complex (Table 1). This suggests a similar affinity of the binding sites localized on the exposed RC protein and on the LDAO ring.

Equilibrium sorption isotherms characterize thermodynamically two main populations of water molecules adsorbed to the RC−detergent complex: those tightly bound at primary hydration sites and those less tightly bound presumably condensing at the surface of the partially hydrated complex when the relative humidity increases. This basic picture is confirmed by the spectral analysis of the intramolecular $(\nu_2 + \nu_3)$ combination band of water, which has been decomposed into three Gaussian sub-bands attributed to subpopulations of water molecules differing in H-bonding organization. Detailed models have been proposed in which the resolved sub-bands have been ascribed to water molecules forming a different number of H bonds with their immediate neighbors[47,59,60] and/or involved in symmetrical or unsymmetrical H bonds of different strength[45] or characterized by a different H-bond connectivity on a larger scale.[61] Despite differences in the structural interpretations, often reflecting different views on the structure/dynamics of liquid water, the lowest frequency sub-band (band 1) can be reasonably attributed to water molecules highly connected through an extended H-bond organization in which each water molecule forms a few H bonds (3−4) with its neighbors, typical of pure, bulk water. The breaking of this structure, leading to distortion of H bonding and weakening of connectivity, typical of small water aggregates and dimers, appears to originate band 2, of intermediate frequency, and the highest frequency band 3, associated with highly disconnected water molecules, possibly involved in a single H bond.[59,60]

In highly hydrated RC−detergent systems the three sub-bands are centered at the same wavenumbers observed in pure water. As in pure water, the bandwidth decreases monotonically from band 1 (centered at the lowest frequency) to band 3 (highest frequency). Such a coincidence is not surprising: under these conditions, as indicated by the Hailwood and Horrobin isotherm, water sorption is largely dominated by weakly bound water molecules, forming a multilayer structure in which the H-bonding organization and energetics are not expected to be significantly perturbed as compared to liquid water. When, according to the Hailwood and Horrobin isotherm, the population of the weakly bound water molecules is decreased, the relative contribution of band 1 (attributed to highly H-bond-connected water structures, typical of bulk water) is also decreased and disappears at relatively low hydration levels ($r < 40\%$), suggesting that a significant fraction of the residual water interacts directly with the RC−detergent complex and that the interaction with the surfactant head groups causes a disruption of the H-bond network present in bulk water. The disappearance of band 1 is in line with the results of a Gaussian analysis of the OH stretching band of water in reverse micelles.[62] This study showed that the contribution of the lowest frequency sub-band decreases from ~50% to ~15% when the $[H_2O]/[\text{detergent}]$ molar ratio (W) is decreased from 12 to 0.4. The lowest frequency Gaussian component prevailing in pure water is closely related to band 1 of the water combination band and is also attributed to water molecules organized in regular structures with unstrained H bonds.[61,62] The vanishing of band 1 observed in RC−detergent films upon dehydration appears therefore to reflect the disappearance of bulk-like water molecules. Interestingly, the decrease of band 2 and increase of band 3 fractional areas observed in RC−detergent films when reducing further the relative humidity to about 10% also resembles the evolution of the corresponding OH stretching sub-bands in reverse micelles characterized by a progressively lower water content.[62] The qualitatively similar behavior observed in RC−detergent films and in reverse surfactant micelles at low hydration levels suggests a progressive reduction of H-bond-connected domains of water molecules adsorbed at the surface of the RC detergent belt. During this evolution of the $(\nu_2 + \nu_3)$ combination band the peak of both bands 2 and 3 shifts to lower wavenumbers, indicating that the H bonds involving the residual populations of adsorbed water become stronger. At $r \leq 6\%$ the contribution of band 2 increases at the expense of band 3, and the peak wavenumber of band 3 undergoes an additional, steep downward shift (Figure 4A and 4B), suggesting further rearrangements of the H-bonding organization at extreme draft. The different structural and dynamical properties of these residual water molecules are also inferred from the impressive narrowing of bands 2 and 3 (Figure 4C), pointing to a dramatic reduction in the number of accessible configurations and H-bond angles for the water molecules most tightly bound to the RC−detergent complex. At such low hydration levels the absolute number of water molecules per complex evaluated from the area of the $(\nu_2 + \nu_3)$ band (<100 at $r = 3\%$) is certainly a very rough estimate, implying the crude assumption that the average oscillator strength weighted over the band is still unaffected by the hydration state of the system. It is however tempting to speculate that under this extreme dryness the inner hydration shell of the complex has been strongly depleted and that even some molecules belonging to highly structured water clusters bound within RC cavities[90] have been possibly removed.

The changes detected at $r < 10\%$ in the $(\nu_2 + \nu_3)$ intramolecular water combination band correlate with the strong alterations of the association band at low hydration (Figure 5). Previous studies performed in lipid liquid-crystalline phases,[65] in saccharide-coated liposomes,[91] as well as in sugar/water and protein/sugar/water amorphous matrices[67] indicate that the intermolecular association band is a sensitive structural probe of the interactions experienced by the water molecules. In particular, Cordone and co-workers[66,67] proposed that the structuring of the association band and the value of the ratio r_A between the area of the association band and that of the $(\nu_2 + \nu_3)$ band give a rough estimate of the relevance of the interaction between water molecules and non-water H-bond-forming groups. The evolution of the association band observed by us in response to dehydration of RC−detergent films is fully consistent with this notion. Both in RC−LDAO and in RC−OG films the association band undergoes an impressive narrowing upon dehydration, but only at $r < 10\%$ a clear structuring of the profile takes place, paralleled by a steep increase of r_A (Table 2). It is noteworthy that the increase of r_A occurs only when, according to the Hailwood and

Horrobin analysis of the hydration isotherms, most of the weakly bound water molecules have been removed. Under these conditions, the different structure of the band in the presence of LDAO and OG indicates that even in the most dried samples (r = 3%) a significant fraction of the residual water is tightly bound to the detergent ring and reflects a different organization of H bonding between residual water molecules and the polar head groups of LDAO and OG.

4.2. Hydration of the RC−Detergent Complex Modulates the RC Dynamics and Stability of the Primary Charge-Separated State. Dehydration of RC−detergent films results in accelerated and broadly distributed kinetics of $P^+Q_A^-$ recombination, in qualitative agreement with previous results.[36] In our previous observations[33,36] we reported effects somewhat variable and weaker than shown in the present paper. In these works the kinetic effects were not correlated with the content of residual water, which could not be determined in extensively dried films due to the low sensitivity of the NIR dispersive spectrometer used to record the combination band of water. In the present study a systematic analysis of $P^+Q_A^-$ recombination kinetics as a function of the hydration level was made possible by (a) use of FTIR spectroscopy to determine the water content of the films and (b) strict control of the hydration level of the RC−detergent films reached by equilibrating them with an atmosphere of defined relative humidity. This approach has shown indeed that large effects on the kinetics of $P^+Q_A^-$ are observed only at very low hydration levels.

The dependence of the average rate constant $\langle k \rangle$ and of the width of the rate distribution σ upon the relative humidity r (Figure 8) shows that both parameters do not change significantly for $0.43 < r < 0.94$, i.e., when the water content is reduced from $\sim 3.5 \times 10^4$ to $\sim 2 \times 10^3$ water molecules per RC−LDAO complex and from $\sim 10^4$ to $\sim 10^3$ water molecules per RC−OG complex. Upon further dehydration $\langle k \rangle$ and σ increase steeply following a sigmoidal dependence. It is noteworthy that $\langle k \rangle$ and σ follow the same dependence upon r in RC−LDAO and RC−OG complexes (see below).

As outlined in the Introduction, these kinetic effects, previously detected upon dehydration of amorphous RC/water/trehalose matrices at room temperature[33−37] and upon freezing RCs in water/glycerol to cryogenic temperatures,[5,13,92,93] can be taken to reflect a strong inhibition of the RC conformational dynamics on the time scale probed by $P^+Q_A^-$ recombination. The increase of the average rate constant $\langle k \rangle$ is taken to indicate an impairment of the RC relaxation from the dark-adapted to the light-adapted conformation, resulting in destabilization of the $P^+Q_A^-$ charge-separated state. The increase in σ is considered to reflect the "freezing" of the interconversion among RC conformational substates, which makes observable the structural and kinetic heterogeneity of the RC population over the time scale of charge recombination.[5,94] The maximal values reached by $\langle k \rangle$ and σ at low hydration levels of the RC−detergent films (corresponding to a few hundreds of water molecules per RC−detergent complex) are quantitatively comparable with those measured in extensively dried RC/water/trehalose matrices at room temperature.[36] Dehydration mimics the effects of freezing the RC complexes in water/glycerol systems[93] at T < 50 K. In the hydrated system upon decreasing the temperature from 200 to 150 K and to 50 K $\langle k \rangle$ increases from ~10 to ~30 s^{-1} and to ~45 s^{-1}, respectively.[93] We infer that an extensive dehydration of the RC−detergent complex brings about a drastic reduction of the RC conformational dynamics, simulating the effects of cryogenic temperatures.

The critical role of hydration water in determining the internal motions and hence the function of globular proteins has been deeply investigated during the last decades (see, e.g., ref 95 and references therein), and it is now well ascertained that a threshold level of hydration is required to fully activate protein dynamics (and functionality).[23] The interplay between solvent and protein dynamics has been rationalized in a "unified model of protein dynamics"[3] which systematizes a large body of experimental and theoretical investigations in myoglobin.[26] Three classes of protein dynamical processes are identified: (a) class I processes, including typically large-scale motions of the protein, driven by thermal fluctuations of the bulk solvent and found to obey dielectric α relaxations; (b) class II processes, e.g., ligand migration inside myoglobin, powered and controlled by the solvent fluctuations of the hydration shell which surrounds the protein and following dielectric β relaxations; (c) class III processes, such as molecular vibrations in the force-field potential of atom−atom interactions not controlled by external fluctuations. In a recent EPR study[37] we applied these concepts to clarify the control exerted on electron transfer kinetics by the protein/solvent environment when RC complexes are embedded into trehalose glasses and poly(vinyl alcohol) matrices. We proposed to ascribe the relaxation of the RC from the dark- to the light-adapted conformation as well as the thermal interconversion between lower tier conformational substates of the RC to Class II processes, slaved to the fluctuations of the hydration shell. This attribution is strongly supported by the results of the present study, which indicate that in the absence of any saccharide or polymeric matrix relaxation from the dark- to the light-adapted conformation is progressively hampered upon removal of water molecules bound to the RC−detergent complex. At very low hydration levels the degree of inhibition of the conformational relaxation is comparable to the one attained at cryogenic temperature in water/glycerol media, as predicted for Class II dynamical processes driven by the β-fluctuations of the hydration shell.[3] It is noteworthy that, as shown by the similar dependence of $\langle k \rangle$ and σ upon the relative humidity, the interconversion among lower tier substates and relaxation from the dark- to the light-adapted conformation are inhibited in parallel when the hydration of the protein complex is reduced. This suggests that the protein conformational fluctuations and the relaxation processes which stabilize the $P^+Q_A^-$ charge-separated state are dynamically coupled, both being driven by the fluctuations of the hydration shell. Interestingly, it has been shown recently that IR bands attributed to water molecules weakly H bonded to the RC are perturbed upon light-induced reduction of Q_A.[96] The dielectric relaxation of these water molecules has been proposed to play an important role in stabilizing the primary charge-separated state.[96]

As already observed, the dependence of $\langle k \rangle$ and σ upon the relative humidity r coincides in RC−LDAO and RC−OG films (Figure 8A and 8B), in spite of the fact that, at any given r value, the amount of water bound to the RC−detergent complex is considerably larger in the presence of LDAO as compared to OG (see the adsorption isotherms in Figure 2). This observation strongly suggests that the hydration state of the detergent belt has a negligible impact on the RC dynamics which govern the kinetics of $P^+Q_A^-$ recombination. Since at any fixed r value the exposed protein will have the same level of hydration, independent of the detergent, we propose therefore that the RC dynamics probed by the recombination kinetics is essentially determined by the hydration state of the exposed protein surface, i.e., of the globular domain of the H subunit and of the hydrophilic portion

of the LM complex which in vivo faces the periplasmic space. We also notice that according to the geometrical model developed to interpret the water sorption results (Figure 9) the area of the exposed protein surface is comparable in the RC−LDAO (7.65×10^3 Å^2) and RC−OG complexes (6.55×10^3 Å^2).

The Hailwood and Horrobin isotherms determined for the RC−LDAO and RC−OG complexes (Figure 2) provide overall thermodynamic parameters for water sorption averaged over the detergent belt and the exposed portion of the RC. However, the hydration state of the exposed protein at a given relative humidity can be roughly estimated by assuming that the affinity K_1 for tight water binding of the exposed RC surface is reasonably approximated by the values which have been determined from a Hailwood and Horrobin analysis of water sorption in soluble proteins.[55] Using the set of proteins already considered in Table 4, the data of ref 55 yield an average affinity $K_1 = 13.8$ with a standard deviation equal to 2.9. By replacing this value in the first term of the Hailwood and Horrobin equation (eq 2) we can easily evaluate the fraction of occupied tight binding sites of the exposed RC surface as a function of the relative humidity r. Inhibition of the RC conformational dynamics, as probed by the increase of $\langle k \rangle$ and σ values, starts at $r \approx 0.4$ (Figure 8). By assuming the K_1 value reported above, at this relative humidity more than 80% of the tight water binding sites of the exposed surface of the RC are expected to be still occupied. The maximum inhibition of the RC conformational dynamics is found at r between 6% and 3% (Figure 8). At these values of relative humidity, 55% and more than 70%, respectively, of the tight water binding sites are predicted to be empty. This behavior indicates that removal of a large part of the hydration shell of the exposed RC protein is needed to arrest the β-slaved RC dynamical processes on the time scale probed by $P^+Q_A^-$ recombination.

The kinetic analysis summarized in Figures 6 and 7 and Table 3 shows that a limited decrease of the amount of residual water (when r decreases from 11% to 9%) leads to the appearance of a second, well-resolved, and much faster phase of charge recombination ($\tau \approx 3 \times 10^2$ μs), suggesting that a sharp structural/dynamical transition has occurred in a large fraction (~50%) of the RC population. Consistently, this strong alteration of the kinetics is paralleled by drastic spectral changes of the residual water, which, as discussed in section 4.1, reflect a strong reduction in the accessible H-bonding configurations of the inner hydration shell. The fast phase is also distributed in rate (Figure 7C and Table 3), indicating that the corresponding RC subpopulation is also frozen over a large ensemble of conformational substates. To our knowledge, such a fast phase of $P^+Q_A^-$ recombination has not been observed previously as a result of environmental alterations, or genetic mutations, or even in RC complexes frozen at 10 K.[5,94] We therefore ascribe this fast recombination to a new conformation produced by removal of specific, tightly bound water molecules, which play a specific structural and/or energetic role in stabilizing the primary light-induced charge-separated state.

In the frame of the semiclassical Marcus model of electron transfer, which is supposed to hold at room temperature, the rate constant of the process is given by[97]

$$k = \frac{4\pi^2}{h} V^2 \frac{1}{\sqrt{4\pi\lambda k_B T}} \exp\left[-\frac{(\varepsilon - \lambda)^2}{\sqrt{4\lambda k_B T}} \right] \quad (13)$$

where ε is the difference in free energy between $P^+Q_A^-$ and PQ_A states, λ is the reorganization energy, V is the electronic interaction matrix element describing the weak coupling between the initial and the final electronic states, k_B and h are the Boltzmann and Planck constants, and T is the absolute temperature. It is generally assumed that, to a reasonable approximation, V^2 falls off exponentially[98] with the distance R, i.e.

$$V^2 = V_0^2 \exp(-\beta R) \quad (14)$$

where $\beta = 1.4$ Å^{-1}. In terms of eqs 13 and 14 an increase in k can be accounted for by a decrease of R, an increase in the free energy difference ε, or a decrease of the reorganization energy λ. It may be instructive to evaluate to which extent a variation in each of these parameters could individually account for the difference between the average rate constant of the slow phase (~50 s^{-1} in LDAO, ~40 s^{-1} in OG) and that of the fast phase (~3500 s^{-1} in LDAO, ~1800 s^{-1} in OG) detected at extreme draft. Equation 14 immediately shows that such an acceleration of the electron transfer process could be caused by a decrease in R equal to 3.0 (in RC−LDAO) and 2.7 Å (in RC−OG complexes). This corresponds to a contraction of about 10% of the distance (28.5 Å) measured between the Q_A ring and the center of a line connecting the Mg atoms of the P dimer (pdb 2J8C).[90] As to the change required in ε or λ to obtain the same kinetic effect, it depends significantly on the values assumed for these two parameters when the reaction proceeds with the rate constant of the slow phase. Estimates of the free energy change associated with the reaction range between 500 and 600 meV.[99] Different approaches yielded the following estimates of the reorganization energy λ (meV): 640,[100] 600 ± 100,[101] 1250,[102] 900,[92,103] 820 ± 30,[104] and 667.[5] By assuming a value of ε between 500 and 600 meV (see above) eq 13 shows that even the largest decrease in the reorganization energy allowed without entering the inverted Marcus region is unable to account for the rate constant of the fast phase, unless the largest estimate (1250 meV) is used for the unperturbed λ. In this case the required decrease in the reorganization energy is ~500 meV. A similar situation holds when the effect of a variation in ε is considered. Again, the effect can be accounted for only by assuming an unperturbed $\lambda = 1250$ meV and a large variation of ε (about 500 meV). It should be considered, however, that an increase of ε, i.e., an increase of the energy level of the $P^+Q_A^-$ state, implies a decrease of the energy difference (ΔG^0_I) between $P^+Q_A^-$ and the intermediate charge-separated state involving the bacteriopheophytin cofactor, P^+BPhe^-. It has been shown[99] that such a decrease allows the thermal repopulation of the intermediate P^+BPhe^- state, activating an indirect pathway of $P^+Q_A^-$ charge recombination, in addition to the direct one. When considering this possibility, the observed rate constant k_{obs} of $P^+Q_A^-$ recombination is given by the rate constant of the direct (tunneling) process, k_{PA} (given by eq 13), plus the contribution of the thermally activated, indirect route,[99] i.e.

$$k_{obs} = k_{PA} + k_{PI} \exp(-\Delta G^\circ_I / k_B T) \quad (15)$$

where $k_{PI} = 8 \times 10^7$ s^{-1} is the rate constant for P^+BPhe^- recombination and $\Delta G^0_I \cong 550$ meV in native RCs.[99] By combining eqs 15 and 13 we can estimate that, assuming intermediate unperturbed values for ε and λ (i.e., 500 and 800 meV, respectively), an increase in ε of about 300 meV (implying $\Delta G^0_I \cong 250$ meV) results in $k_{obs} \cong 3.7 \times 10^3$ s^{-1}, a value comparable to that measured for the fast phase of $P^+Q_A^-$ recombination in dehydrated RC−LDAO complexes. In other words, a limited destabilization of the $P^+Q_A^-$ state can result in a strong acceleration of

charge recombination, due to activation of the indirect route through the P^+BPhe^- state.

The three different effects considered could cooperate in determining the fast recombination kinetics observed under extreme dehydration. In fact, it is plausible that removal of water molecules bound at specific sites and orientations inside the RC complex can affect the electrostatics of the P and Q_A cofactors environment, increasing the value of ε and decreasing the value of the reorganization energy for the direct recombination, due to a decrease in the number (and mobility) of interacting solvent dipoles. At the same time, it is not unreasonable that the RC, upon partial depletion of water molecules in its cavities and clefts, responds with a structural shrinking which might affect the distance between P^+ and Q_A^-. Remarkably, this strong destabilization of the charge-separated state, possibly involving significant structural rearrangements, is fully reverted upon rehydration of the RC−detergent films.

Finally, the effects of dehydration observed in RC−detergent films as compared to the ones previously reported for RC−water−trehalose glassy matrices[33−37] deserve some comments. Except for the presence of an additional, much faster kinetic phase of $P^+Q_A^-$ recombination, which was not detected in RC−trehalose glasses, dehydration leads in both systems to a comparable increase of $\langle k \rangle$ and σ of $P^+Q_A^-$ recombination, which indicates a restriction of the associated conformational dynamics. This similarity might cast some doubts on the effective role of trehalose and the glassy state of the RC−water−sugar matrix in controlling the RC internal dynamics, which might be suspected to simply arise from dehydration of the RC−detergent complex also in the presence of trehalose. We have at variance proposed that trehalose takes an active and a peculiar role in conditioning the protein dynamics through formation of a network of H bonds interconnecting sugar molecules of the rigid glassy matrix with water molecules of the hydration shell which are in turn H bonded to surface groups at the protein.[35,38] This results in a strong slaving of the protein dynamics to that of the glassy matrix. A comparison of the water contents of the samples at which the kinetic effects on $P^+Q_A^-$ recombination become observable in the absence and presence of trehalose does not provide relevant information, because the trehalose matrix itself (formed by approximately 10^4 sugar molecules per RC) binds a considerable amount of water, even under extremely dehydrating conditions; consistently, the discussed kinetic effects are observed in the presence of trehalose at higher H_2O/RC molar ratios ($\sim 10^4$)[33,35,36] as compared to RC films without sugar (H_2O/RC $\approx 10^3$). The following two observations, however, mark important structural and dynamical differences in the two systems: (a) as previously reported[35] and verified in this work under controlled, extreme dehydration, in RC−detergent films the primary photochemistry is irreversibly suppressed and the RC bacteriochlorin cofactors lose their native coordination after about 3 days of incubation at 37 °C; the thermal stability of the RC is tremendously enhanced in the trehalose matrix, where on the contrary no degradation occurs even after several days of incubation at 37 °C;[35] (b) in extensively dehydrated RC−trehalose glassy matrices $P^+Q_A^-$ recombination after a few seconds of continuous, intense photoexcitation is only slightly decelerated as compared to the one recorded after a laser flash, indicating that a prolonged permanence of the system in the charged-separated state can remove only partially the matrix-induced inhibition of the conformational relaxation.[34] At variance, in extensively dried RC films a comparable period of continuous illumination leads to a total recovery of the kinetics observed in the fully hydrated system, indicating that the impairment of the conformational protein dynamics induced by dehydration is less severe than in the glassy matrix and can be totally removed upon continuous photoexcitation.[105] This different behavior suggests that the inhibition mechanism of the RC dynamics, although involving in both cases the hydration shell of the RC−detergent complex, is different in the two systems and that in the presence of trehalose the protein dynamics is inhibited because it is tightly slaved to that of the embedding glassy matrix.

5. CONCLUDING REMARKS

The reported results show that the hydration state of a large protein−detergent complex as the photosynthetic reaction center can be reversibly varied and controlled over a wide range, providing a tool to modulate the internal protein dynamics at room temperature and to explore the protein−solvent dynamical coupling. The concomitant analysis of $P^+Q_A^-$ recombination kinetics and of water sorption equilibrium points to the following main conclusions.

(i) At least two populations of adsorbed water molecules can be resolved on a thermodynamic and spectral basis, i.e., weakly and tightly bound water; the comparison between RC−LDAO and RC−OG complexes reveals that a substantial fraction of the tight hydration shell interacts with the polar headgroups of the detergent micelle surrounding the RC.

(ii) A minimum hydration level of the complex is required to allow a fast relaxation from the unstabilized dark-adapted to the stabilized light-adapted conformation of the charge-separated $P^+Q_A^-$ state as well as fast interconversion among lower tier conformational substates of the RC over the time scale (0.1 s) of charge recombination. More specifically, these RC dynamics appear to be governed by the hydration state of the exposed RC surface, not screened by the detergent belt. When this protein hydration shell is depleted inhibition of the RC relaxation and substates interconversion is comparable to that observed at cryogenic temperature in the hydrated system.

(iii) Removal of a limited pool of hydration water, belonging to the most tightly bound population and including highly structured water molecules, possibly located inside RC cavities, accelerates charge recombination by 2 orders of magnitude.

As a whole the results strongly support the notion that relaxation of the RC from the dark-adapted to the light-adapted conformation as well as the interconversion among lower tier conformational substates are β-slaved processes driven and controlled by the dynamics of the protein hydration shell. Inner water molecules tightly bound to the RC further stabilize the primary charge-separated state by affecting the structure and/or the electrostatics of the complex.

APPENDIX

A formula is derived for calculation of the surface area of an ellipsoidal ring, formed by revolution of an ellipse of semiaxes a and b around a cylindrical core of radius R, with axis along x. The area element dA of the surface of revolution obtained by rotating the arc segment ds of curve $f(x)$ about

the x axis is

$$dA = 2\pi f(x)ds = 2\pi f(x)\sqrt{1 + [f'(x)]^2}dx$$

so that the surface area A obtained by rotating the arc between $x = -a$ and $x = +a$ will be

$$A = 2\pi \int_{-a}^{+a} f(x)\sqrt{1 + [f'(x)]^2}\, dx \quad \text{(A1)}$$

For the described ellipsoidal ring, the function to be evaluated is

$$f(x) = R + y$$

where y obeys the equation of the ellipse

$$\frac{x^2}{a^2} + \frac{y^2}{b^2} = 1$$

so that

$$f(x) = R + \frac{b}{a}(a^2 - x^2)^{1/2} \quad \text{(A2)}$$

After taking the derivative of eq A2, replacing in eq A1, and rearranging, we obtain

$$A = \frac{2\pi b}{a}\int_{-a}^{+a}\left[a^2 - \frac{x^2}{a^2}(a^2 - b^2)\right]^{1/2} dx + 2\pi R\int_{-a}^{+a}\left[1 + \frac{b^2x^2}{a^2(a^2 - x^2)}\right]^{1/2} dx \quad \text{(A3)}$$

AUTHOR INFORMATION

Corresponding Author

*Phone: +39-051-2091288. Fax: +39-051-242576. E-mail: giovanni.venturoli@unibo.it.

ACKNOWLEDGMENT

The authors thank L. Cordone (Palermo University), G. Palazzo (Bari University), K. Möbius (Free University, Berlin), A. Savitsky, and W. Lubitz (Max Planck Institute for Bioinorganic Chemistry, Mülheim an der Ruhr) for stimulating, clarifying discussions. The authors are also grateful to C. Degli Esposti (Bologna University) and A. Mezzetti (CEA-Saclay, Gif-sur-Yvette) for useful advices in the analysis of FTIR spectra. Financial support from MIUR of Italy (Grant PRIN 2008ZWHZJT) is gratefully acknowledged.

REFERENCES

(1) Henzler-Wildman, K.; Kern, D. *Nature* **2007**, *450*, 964–972.
(2) Frauenfelder, H.; Sligar, S. G.; Wolynes, P. G. *Science* **1991**, *254*, 1598–1603.
(3) Frauenfelder, H.; Chen, G.; Berendzen, J.; Fenimore, P. W.; Jansson, H.; McMahon, B. H.; Stroe, I. R.; Swenson, J.; Young, R. D. *Proc. Natl. Acad. Sci. U.S.A.* **2009**, *106*, 5129–5134.
(4) Frauenfelder, H.; McMahon, B. H.; Fenimore, P. W. *Proc. Natl. Acad. Sci. U.S.A.* **2003**, *100*, 8615–8617.
(5) McMahon, B. H.; Müller, J. D.; Wraight, C. A.; Nienhaus, G. U. *Biophys. J.* **1998**, *74*, 2567–2587.
(6) Wöhri, A. B.; Katona, G.; Johansson, L. C.; Fritz, E.; Malmerberg, E.; Andersson, M.; Vincent, J.; Eklund, M.; Cammarata, M.; Wulff, M.; Davidsson, J.; Groenhof, G.; Neutze, R. *Science* **2010**, *328*, 630–633.
(7) Feher, G.; Allen, J. P.; Okamura, M. Y.; Rees, D. C. *Nature* **1989**, *33*, 111–116.
(8) Hoff, A. J.; Deisenhofer *J. Phys. Rep.* **1997**, *287*, 1–247.
(9) McElroy, J. D.; Mauzerall, D. C.; Feher, G. *Biochim. Biophys. Acta* **1974**, *333*, 261–278.
(10) Wang, H.; Lin, S.; Allen, J. P.; Williams, J. A.; Blankert, S.; Laser, C.; Woodbury, N. W. *Science* **2007**, *316*, 747–750.
(11) Graige, M. S.; Feher, G.; Okamura, M. Y. *Proc. Natl. Acad. Sci. U.S.A.* **1998**, *95*, 11679–11684.
(12) Arata, H.; Parson, W. W. *Biochim. Biophys. Acta* **1981**, *636*, 70–81.
(13) Kleinfeld, D.; Okamura, M. Y.; Feher, G. *Biochemistry* **1984**, *23*, 5780–5786.
(14) Nabedryk, E.; Bagley, K. A.; Thibodeau, D. L.; Bauscher, M.; Mäntele, W.; Breton, J. *FEBS Lett.* **1990**, *266*, 59–62.
(15) Brzezinski, P.; Andreasson, L. E. *Biochemistry* **1995**, *34*, 7498–7506.
(16) Dzuba, S. A.; Gast, P.; Hoff, A. J. *Chem. Phys. Lett.* **1997**, *268*, 273–279.
(17) Chen, L. X.; Utschig, L. M.; Schlesselman, S. L.; Tiede, D. M. *J. Phys. Chem. B* **2004**, *108*, 3912–3924.
(18) Paddock, M. L.; Flores, M.; Isaacson, R.; Chang, C.; Abresch, E. C.; Okamura, M. Y. *Biochemistry* **2007**, *46*, 8234–8243.
(19) Goushcha, A. O.; Kharkyanen, V. N.; Scott, G. W.; Holzwarth, A. R. *Biophys. J.* **2000**, *79*, 1237–1252.
(20) Andréasson, U.; Andréasson, L.-E. *Photosynth. Res.* **2003**, *75*, 223–233.
(21) Stowell, M. H.; McPhillips, T. M.; Rees, D. C.; Soltis, S. M.; Abresch, E.; Feher, G. *Science* **1997**, *276*, 812–816.
(22) Katona, G.; Snijder, A.; Gourdon, P.; Andréasson, U.; Hansson, Ö.; Andréasson, L.-E.; Neutze, R. *Nat. Struct. Mol. Biol.* **2005**, *12*, 630–631.
(23) Rupley, J. A.; Careri, G. *Adv. Protein Chem.* **1991**, *41*, 37–172.
(24) Tarek, M.; Tobias, D. J. *Biophys. J.* **2000**, *79*, 3244–3267.
(25) Helms, V. *Chem. Phys. Chem.* **2007**, *8*, 23–33.
(26) Fenimore, P. W.; Frauenfelder, H.; McMahon, B. H.; Young, R. D. *Proc. Natl. Acad. Sci. U.S.A.* **2004**, *101*, 14408–14413.
(27) Bizzarri, A. R.; Cannistraro, S. *J. Phys. Chem. B* **2002**, *106*, 6617–6633.
(28) Nakasako, M. *Philos. Trans. R. Soc. London B* **2004**, *359*, 1191–1206.
(29) Halle, B. *Philos. Trans. R. Soc. London B* **2004**, *359*, 1207–1224.
(30) Leitner, D. M.; Gruebele, M.; Havenith, M. *HFSP J.* **2008**, *2*, 314–323.
(31) Clayton, R. K. *Biochim. Biophys. Acta* **1978**, *504*, 255–264.
(32) Nikolaev, G. M.; Knox, P. P.; Kononenko, A. A.; Grishanova, N. P.; Rubin, A. B. *Biochim. Biophys. Acta* **1980**, *590*, 194–201.
(33) Palazzo, G.; Mallardi, A.; Hochkoeppler, A.; Cordone, L.; Venturoli, G. *Biophys. J.* **2002**, *82*, 558–568.
(34) Francia, F.; Palazzo, G.; Mallardi, A.; Cordone, L.; Venturoli, G. *Biochim. Biophys. Acta* **2004**, *1658*, 50–57.
(35) Francia, F.; Dezi, M.; Mallardi, A.; Palazzo, G.; Cordone, L.; Venturoli, G. *J. Am. Chem. Soc.* **2008**, *130*, 10C240–10246.
(36) Francia, F.; Malferrari, M.; Sacquin-Mora, S.; Venturoli, G. *J. Phys. Chem. B* **2009**, *113*, 10389–10398.
(37) Savitsky, A.; Malferrari, M.; Francia, F.; Venturoli, G.; Möbius, K. *J. Phys. Chem. B* **2010**, *114*, 12729–12743.
(38) Cordone, L.; Cottone, G.; Giuffrida, S.; Palazzo, G.; Venturoli, G.; Viappiani, C. *Biochim. Biophys. Acta* **2005**, *1749*, 252–281.
(39) Baciou, L.; Michel, H. *Biochemistry* **1995**, *34*, 7967–7972.
(40) Greenspan, L. *J. Res. Natl. Bur. Stand. A* **1977**, *814*, 89–96.
(41) Sloten, L. *Biochim. Biophys. Acta* **1972**, *275*, 208–218.
(42) Bowyer, J. R.; Meinhardt, S. W.; Tierney, G. V.; Crofts, A. R. *Biochim. Biophys. Acta* **1981**, *635*, 167–186.
(43) Wraight, C. A.; Cogdell, R. J.; Clayton, R. K. *Biochim. Biophys. Acta* **1975**, *396*, 242–249.

(44) Bevington, P. R. *Data Reduction and Error Analysis for the Physical Sciences*; McGraw-Hill: New York, 1969.
(45) Bonner, O. D.; Choi, Y. S. *J. Phys. Chem.* **1974**, *78*, 1727–1731.
(46) Dickens, B.; Dickens, S. H. *J. Res. Natl. Inst. Stan.* **1999**, *104*, 173–183.
(47) Fornés, V.; Chaussidon, J. *J. Chem. Phys.* **1978**, *68*, 4667–4671.
(48) Giustini, M.; Palazzo, G.; Colafemmina, G.; Della Monica, M.; Giomini, M.; Ceglie, A. *J. Phys. Chem.* **1996**, *100*, 3190–3198.
(49) Straley, S. C.; Parson, W. W.; Mauzerall, D. C.; Clayton, R. K. *Biochim. Biophys. Acta* **1973**, *305*, 597–609.
(50) Nabedryk, E.; Tiede, D. M.; Dutton, P. L.; Breton, J. *Biochim. Biophys. Acta* **1982**, *682*, 273–280.
(51) Giguère, P. A.; Chin, D. *Can. J. Chem.* **1961**, *39*, 1214–1220.
(52) Hecht, K. T.; Wood, D. L. *Proc. R. Soc. London, Ser. A* **1956**, *235*, 174–183.
(53) Vandermeulen, D. L.; Ressler, N. *Arch. Biochem. Biophys.* **1980**, *199*, 197–205.
(54) Careri, G.; Giansanti, A.; Gratton, E. *Biopolymers* **1979**, *18*, 1187–1203.
(55) Lüscher-Mattli, M.; Rüegg, M. *Biopolymers* **1982**, *21*, 403–418.
(56) Hailwood, A. J.; Horrobin, S. *Trans. Faraday Soc.* **1946**, *42B*, 84–99.
(57) Bonner, O. D.; Choi, Y. S. *J. Phys. Chem.* **1974**, *78*, 1723–1727.
(58) Czarnik-Matusewicz, B.; Pilorz, S. *Vib. Spectrosc.* **2006**, *40*, 235–245.
(59) Malsam, J.; Aksan, A. *J. Phys. Chem. B* **2009**, *113*, 6792–6799.
(60) Takeuchi, M.; Martra, G.; Coluccia, S.; Anpo, M. *J. Phys. Chem. B* **2005**, *109*, 7387–7391.
(61) Brubach, J.-B.; Mermet, A.; Filabozzi, A.; Gerschel, A.; Roy, P. *J. Chem. Phys.* **2005**, *122*, 184509.
(62) Onori, G.; Santucci, A. *J. Phys. Chem.* **1993**, *97*, 5430–5434.
(63) Kawai, T.; Umemura, J.; Takenaka, T.; Kodama, M.; Seki, S. J. *J. Colloid Interface Sci.* **1985**, *103*, 56–61.
(64) Eisenberg, D.; Kauzmann, W. *The Structure and Properties of Water*; Oxford University Press: London, 1969.
(65) Nilsson, A.; Holmgren, A.; Lindblom, G. *Biochemistry* **1991**, *30*, 2126–2133.
(66) Giuffrida, S.; Cottone, G.; Librizzi, F.; Cordone, L. *J. Phys. Chem. B* **2003**, *107*, 13211–13217.
(67) Giuffrida, S.; Cottone, G.; Cordone, L. *Biophys. J.* **2006**, *91*, 968–980.
(68) Zelent, B.; Nucci, N. V.; Vanderkooi, J. M. *J. Phys. Chem. A* **2004**, *108*, 11141–11150.
(69) Francia, F.; Giachini, L.; Palazzo, G.; Mallardi, A.; Boscherini, F.; Venturoli, G. *Bioelectrochemistry* **2004**, *63*, 73–77.
(70) Steinbach, P. J.; Chu, K.; Frauenfelder, H.; Johnson, J. B.; Lamb, D. C.; Nienhaus, G. U.; Sauke, T. B.; Young, R. D. *Biophys. J.* **1992**, *61*, 235–245.
(71) Brunauer, S.; Emmet, P. H.; Teller, E. *J. Am. Chem. Soc.* **1938**, *60*, 309–319.
(72) Kuntz, I. D.; Kauzmann, W. *Adv. Protein Chem.* **1974**, *28*, 239–345.
(73) D'Arcy, R. L.; Watt, I. C. *Trans. Faraday Soc.* **1970**, *66*, 1236–1245.
(74) Rivas, E.; Reiss-Husson, F.; Le Maire, M. *Biochemistry* **1980**, *19*, 2943–2950.
(75) Møller, J. V.; le Maire, M. *J. Biol. Chem.* **1993**, *268*, 18659–18672.
(76) Gast, P.; Hemelrijk, P. W.; van Gorkom, H. J.; Hoff, A. J. *Eur. J. Biochem.* **1996**, *239*, 805–809.
(77) Roth, M.; Lewit-Bentley, A.; Michel, H.; Deisenhofer, J.; Huber, R.; Oesterhelt, D. *Nature* **1989**, *340*, 659–662.
(78) Roth, M.; Arnoux, B.; Ducruix, A.; Reiss-Husson, F. *Biochemistry* **1991**, *30*, 9403–9413.
(79) Timmins, P. A.; Hauk, J.; Wacker, T.; Welte, W. *FEBS Lett.* **1991**, *280*, 115–120.
(80) Thiyagarajan, P.; Tiede, D. M. *J. Phys. Chem.* **1994**, *98*, 10343–10351.
(81) Yeates, T. O.; Komiya, H.; Rees, D. C.; Allen, J. P.; Feher, G. *Proc. Natl. Acad. Sci. U.S.A.* **1987**, *84*, 6438–6442.
(82) Wolfram, S. *The Mathematica book*; Wolfram Media/Cambridge University Press: New York, 1999.
(83) Rojas, O. J.; Neuman, R. D.; Claesson, P. M. *J. Phys. Chem. B* **2005**, *109*, 22440–22448.
(84) Lorenz, C. D.; Hsieh, C.-M.; Dreiss, C. A.; Lawrence, M. J. *Langmuir* **2011**, *27*, 546–553.
(85) Konidala, P.; He, L.; Niemeyer, B. *J. Mol. Graphics Modell.* **2006**, *25*, 77–86.
(86) Kocherbitov, V.; Veryazov, V.; Söderman, O. *J. Mol. Struct.: THEOCHEM* **2007**, *808*, 111–118.
(87) Curtiss, L. A.; Frurip, D. J.; Blander, M. *J. Chem. Phys.* **1979**, *71*, 2703–2711.
(88) Feyereisen, M. W.; Feller, D.; Dixon, D. A. *J. Phys. Chem.* **1996**, *100*, 2993–2997.
(89) Suzuki, T. *Phys. Chem. Chem. Phys.* **2008**, *10*, 96–105.
(90) Koepke, J.; Krammer, E.-M.; Klingen, A. R.; Sebban, P.; Ullmann, G. M.; Fritzsch, G. *J. Mol. Biol.* **2007**, *371*, 396–409.
(91) Chiantia, S.; Giannola, L. I.; Cordone, L. *Langmuir* **2005**, *21*, 4108–4116.
(92) Ortega, J. M.; Mathis, P.; Williams, J. C.; Allen, J. P. *Biochemistry* **1996**, *35*, 3354–3361.
(93) Kriegl, J. M.; Nienhaus, G. U. *Proc. Natl. Acad. Sci. U.S.A.* **2004**, *101*, 123–128.
(94) Kriegl, J. M.; Forster, F. K.; Nienhaus, G. U. *Biophys. J.* **2003**, *85*, 1851–1870.
(95) Mattos, C. *Trends Biochem. Sci.* **2002**, *27*, 203–208.
(96) Iwata, T.; Paddock, M. L.; Okamura, M. Y.; Kandori, H. *Biochemistry* **2009**, *48*, 1220–1229.
(97) Marcus, R. A.; Sutin, N. *Biochim. Biophys. Acta* **1985**, *811*, 265–322.
(98) Moser, C. C.; Keske, J. M.; Warncke, K.; Farid, R. S.; Dutton, P. L. *Nature* **1992**, *355*, 796–802.
(99) Gopher, A.; Blatt, Y.; Schönfeld, M.; Okamura, M. Y.; Feher, G.; Montal, M. *Biophys. J.* **1985**, *48*, 311–320.
(100) Feher, G.; Arno, T. R.; Okamura, M. Y. In *The Photosynthetic Bacterial Reaction Center*; Breton, J., Vermeglio, A., Eds.; Plenum Press: New York, 1988; pp 271−287.
(101) Gunner, M. R.; Dutton, P. L. *J. Am. Chem. Soc.* **1989**, *111*, 3400–3412.
(102) Franzen, S.; Boxer, S. G. *J. Phys. Chem.* **1993**, *97*, 6304–6318.
(103) Lin, X.; Murchison, H. A.; Nagarajan, V.; Parson, W. W.; Allen, J. P.; Williams, J. C. *Proc. Natl. Acad. Sci. U.S.A.* **1994**, *91*, 10265–10269.
(104) Allen, J. P.; Williams, J. C.; Graige, M. S.; Paddock, M. L.; Labahn, A.; Feher, G.; Okamura, M. Y. *Photosynth. Res.* **1998**, *55*, 227–233.
(105) Malferrari, M.; Francia, F.; Venturoli, G. Manuscript in preparation.